Lewis R Cent.
E A Bourke

STRESS INTENSITY FACTORS FOR SURFACE FLAWED FRACTURE SPECIMENS

QUARTERLY STATUS REPORT

September 30, 1970

Principal Investigator

F. W. Smith

Associate Professor
Department of Mechanical Engineering
Colorado State University
Fort Collins, Colorado

Grant No.

NGR-06-002-063

THEORETICAL WORK

Personnel

R. W. Thresher has completed his work on the contract and has received his Ph.D. No student is presently employed on the theoretical portion of the work.

Progress

The computer program has been run several times for the case of uniform loading on the crack shown in Figure 1. Stress intensity factors have been computed for values of D ranging from D = 0.0 to D = 0.7 and for values of A/T ranging from A/T = 0.0 to A/T = 0.85.

The results of these computations are presented in Dr. Thresher's thesis, a copy of which is attached. Figures 6, 12, 13 and 14 present stress intensity as a function of position along the crack border. Figure 15 presents the back surface magnification factor as a function of A/T. Comparisons of theoretical and experimental work are shown in Figures 16 and

EXPERIMENTAL WORK

Personnel

A master's degree candidate has been hired 1/2 time to work on this portion of the research.

Progress

Testing has continued on the width effect. In excess of 60 data points have been added to the data presented in the last report. Figures 2 through

11 show all the width effect data taken to date. The hollow points show the most recent data while the solid points show the data presented in the last report.

The apparent $K_{IC}(AK_{IC})$ in Figures 2 through 11 is still defined as

$$A_{KIC} = M_1\sigma\sqrt{\frac{\pi a}{Q}}$$

Now that enough data are avilable, a new apparent K_{IC} will be defined, namely

$$AK'_{IC} = M_1M_2\bar{\sigma}\sqrt{\frac{\pi a}{Q}}$$

as was discussed in the last report. This new apparent K_{IC} will be used to compute width effect correction factors.

In the last report it was mentioned that the width effect may have influenced some of the depth effect data. It appears now that this is not the case since the depth effect specimens were purposely made with large values of W/2C. The following criterion were applied to the depth effect data:

invalid if

$$W/2C \leq 4.0 \quad \text{and} \quad a/2C \geq .30$$

$$W/2C \leq 2.0 \quad \text{and} \quad a/2C \leq .30$$

This resulted in eliminating only four of the total depth effect data points.

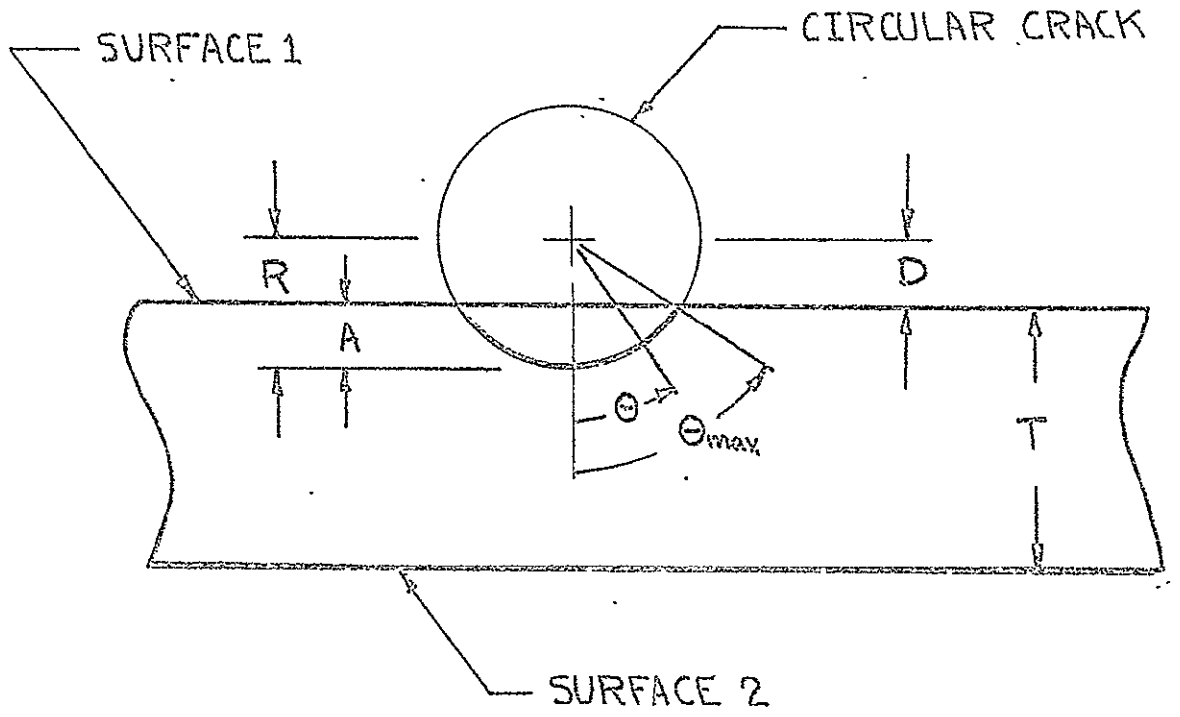

FIGURE 1

FIGURE 2

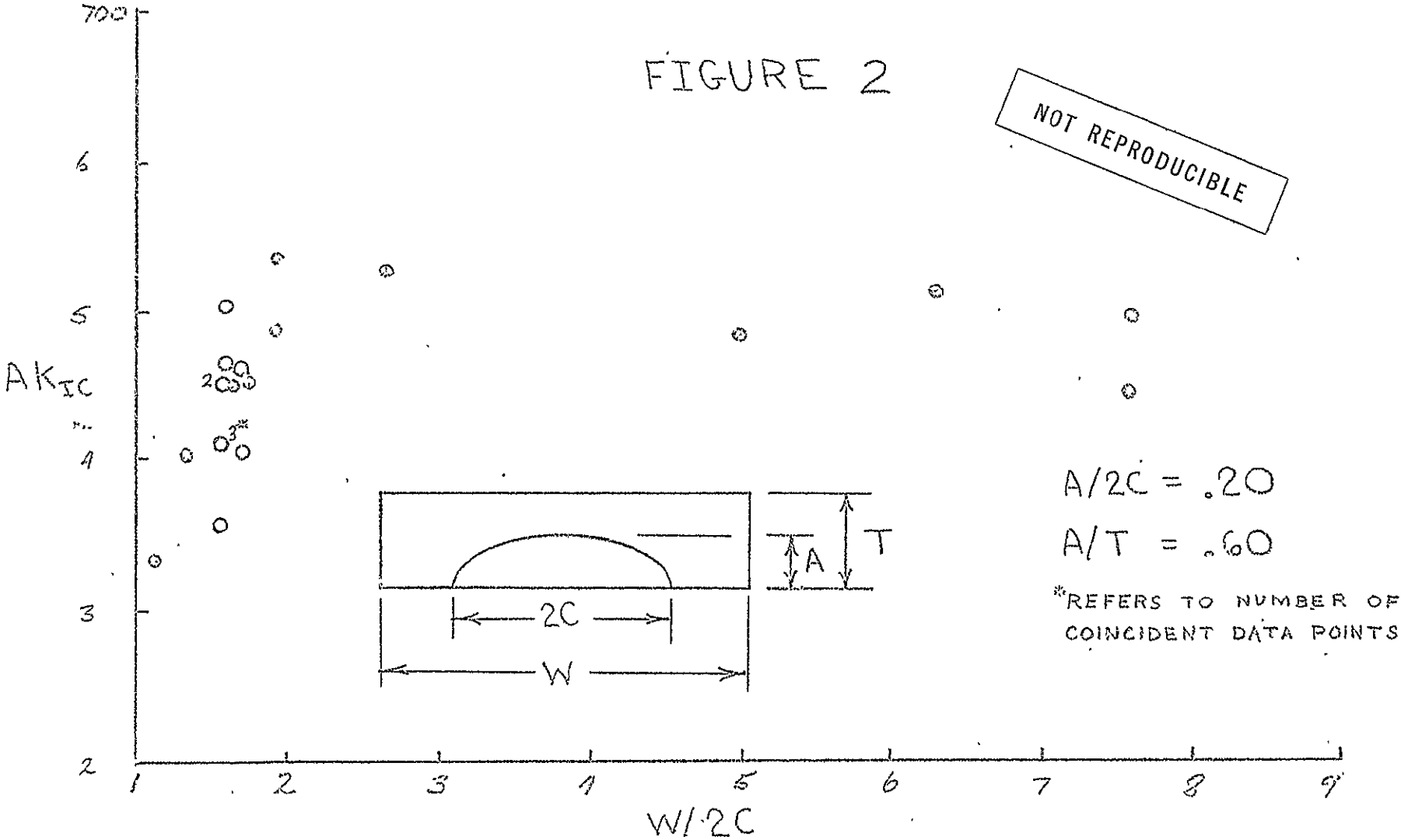
NOT REPRODUCIBLE
700
6
5
4
3
2
AK_{IC}
1
2
3
4
5
6
7
8
9
W/2C
2C
W
A
T
A/2C = .20
A/T = .60
*REFERS TO NUMBER OF COINCIDENT DATA POINTS

FIGURE 3

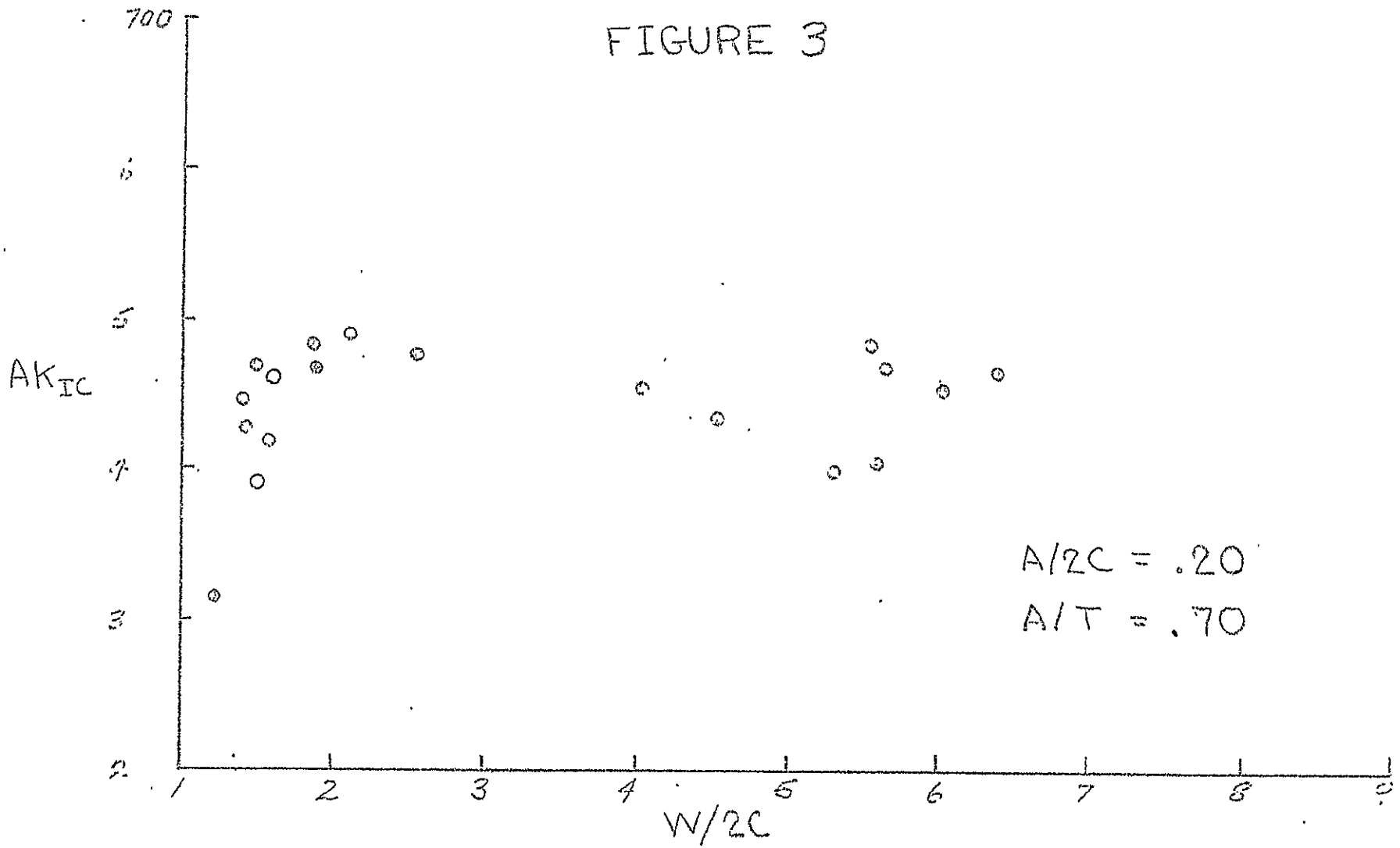

FIGURE 4

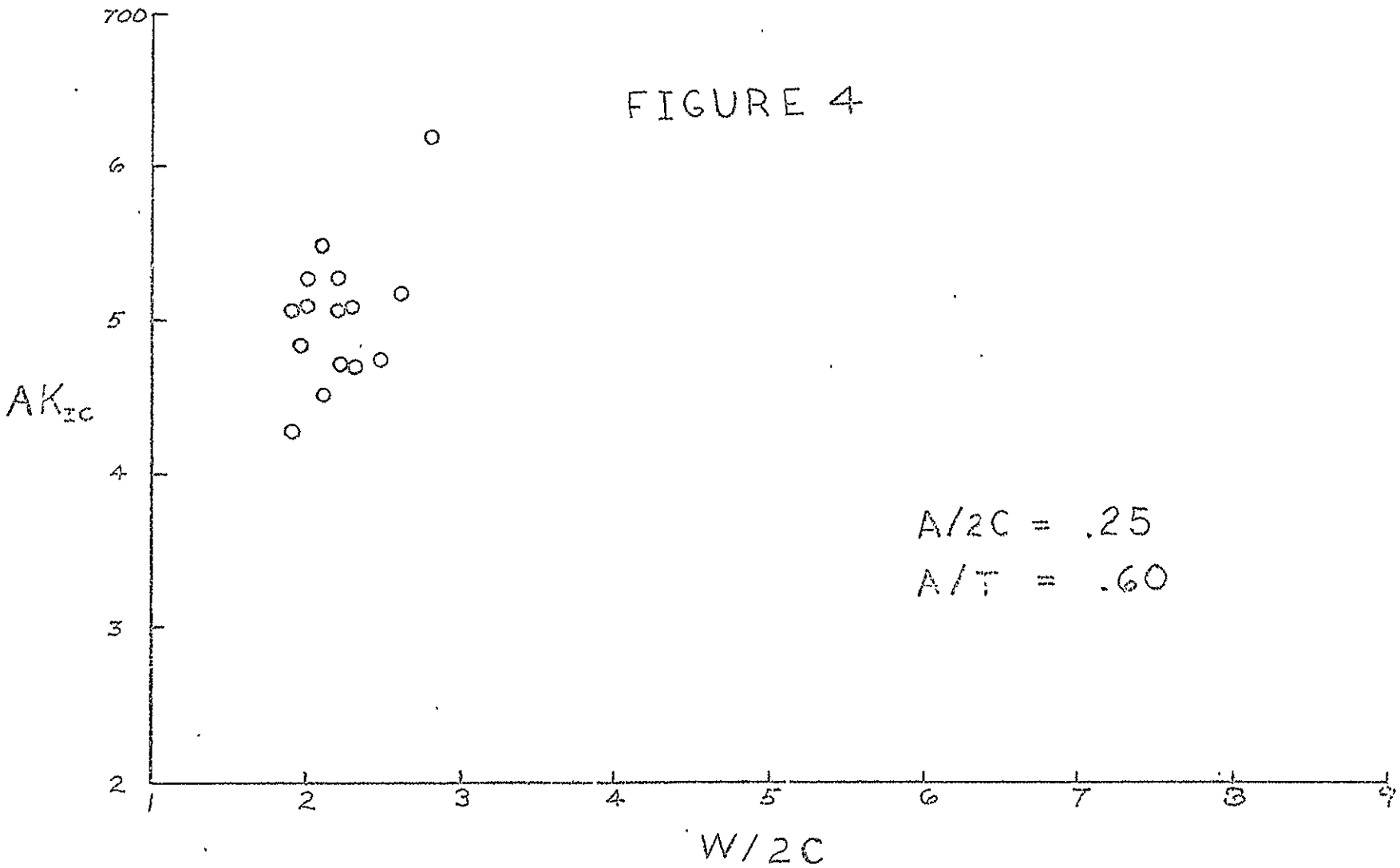

FIGURE 5

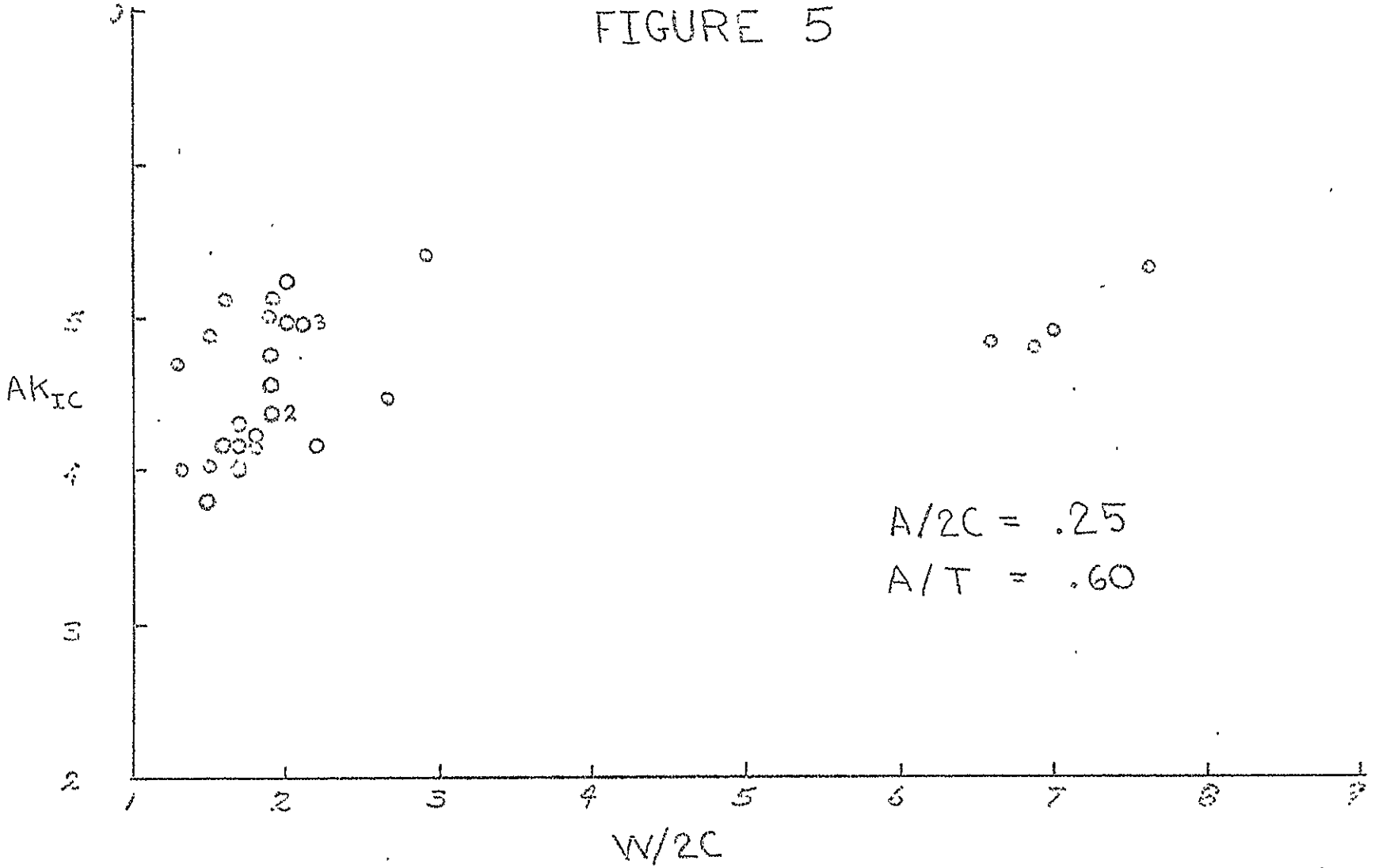

FIGURE 6

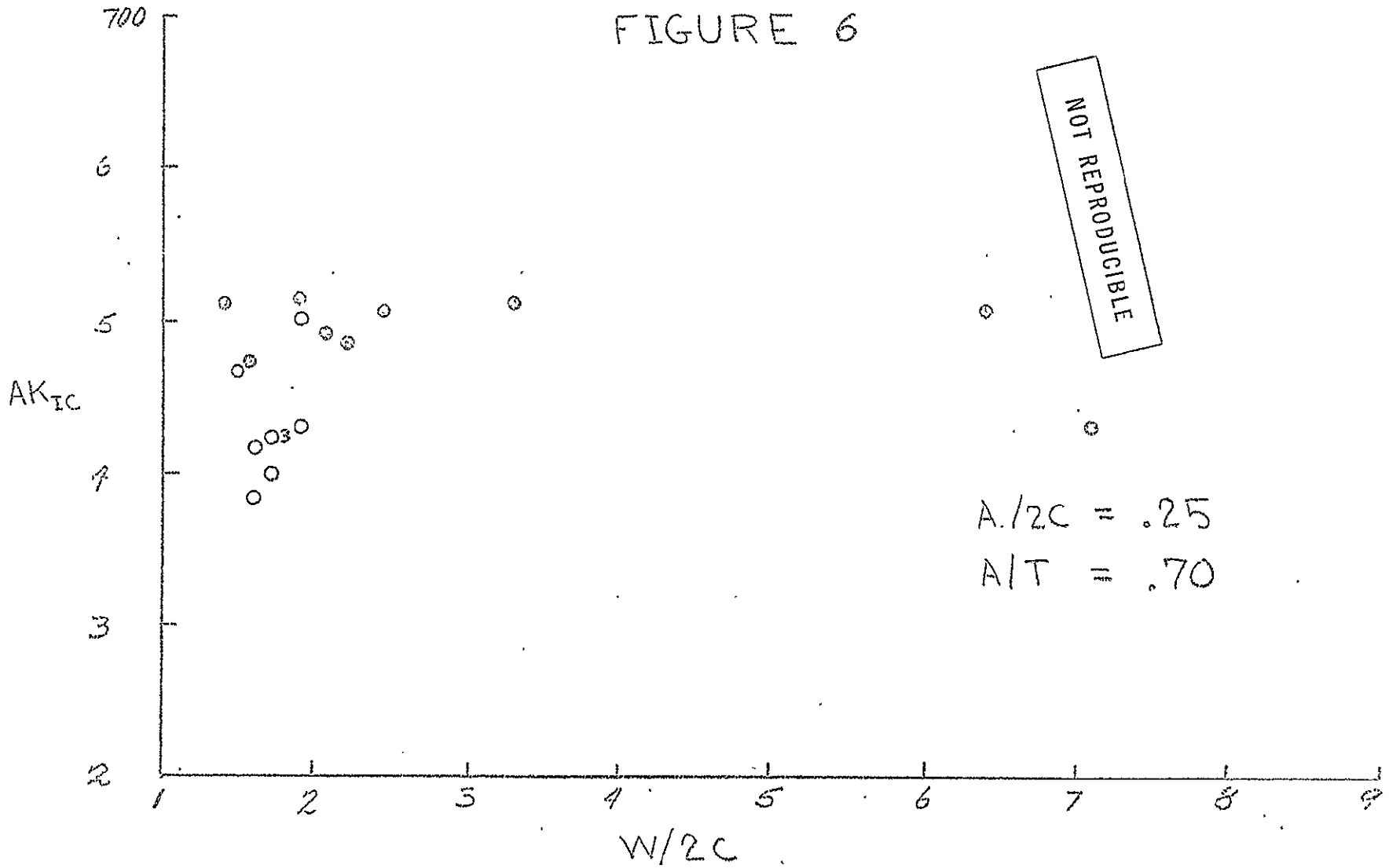

FIGURE 7

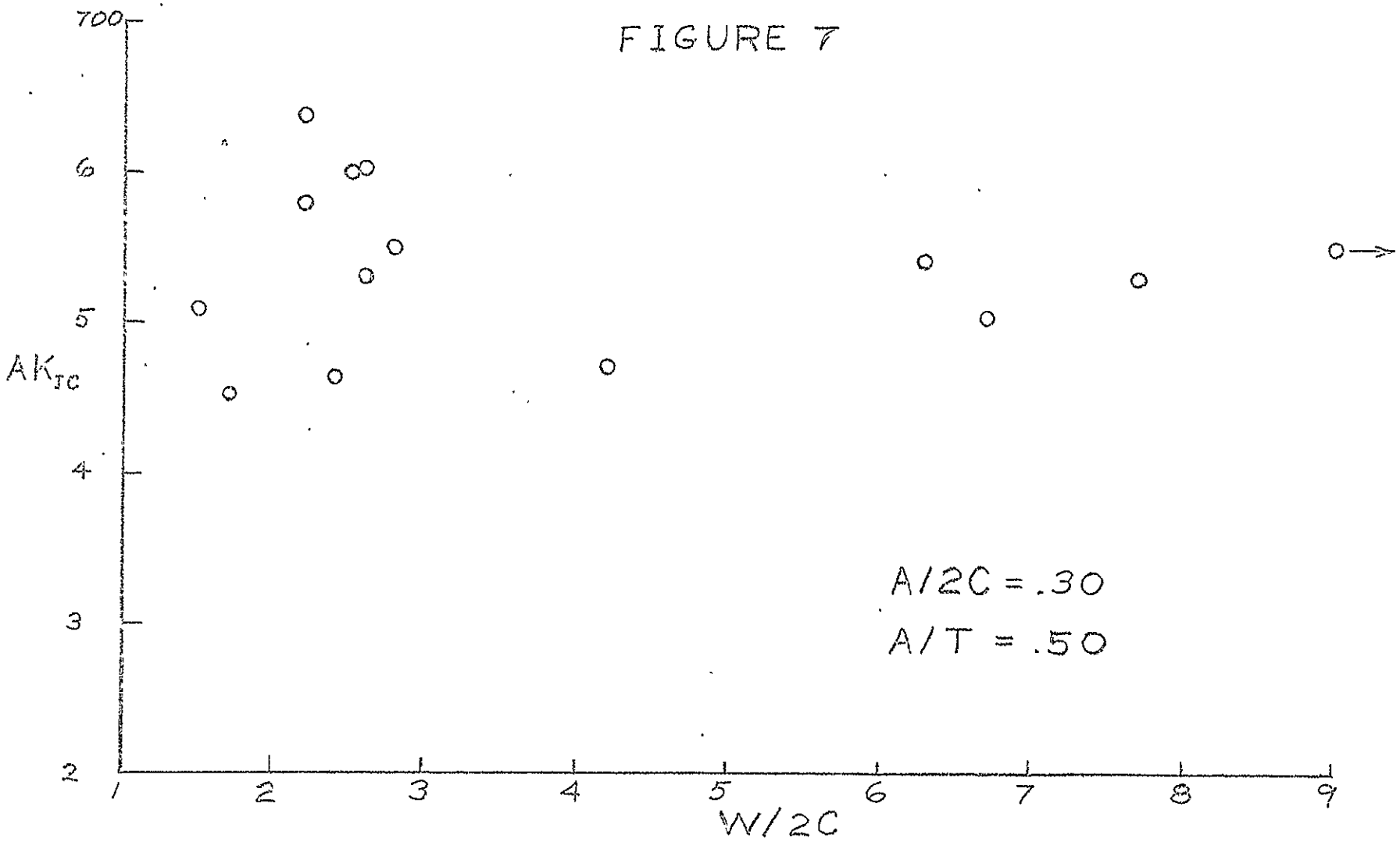

FIGURE 8

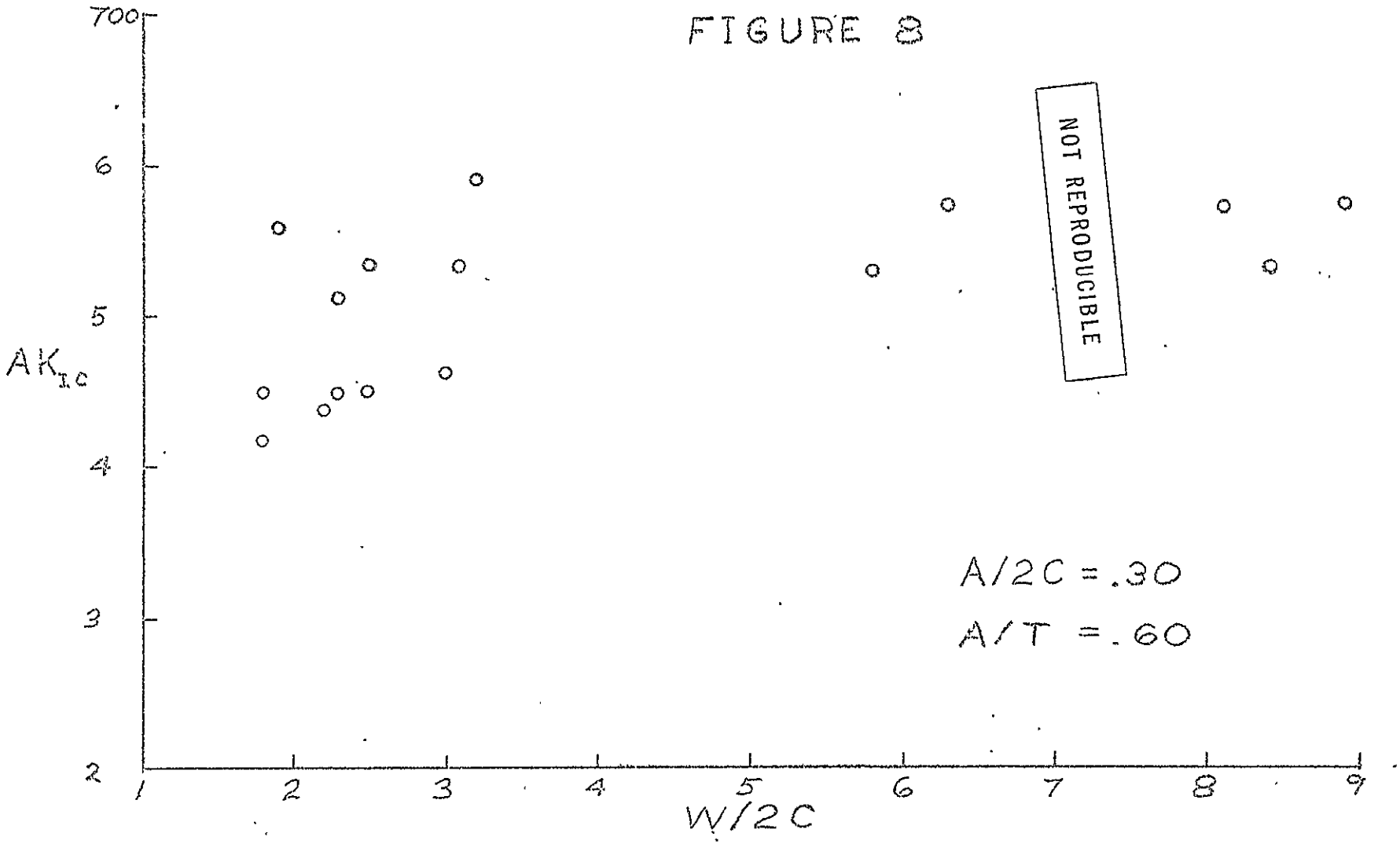

FIGURE 9

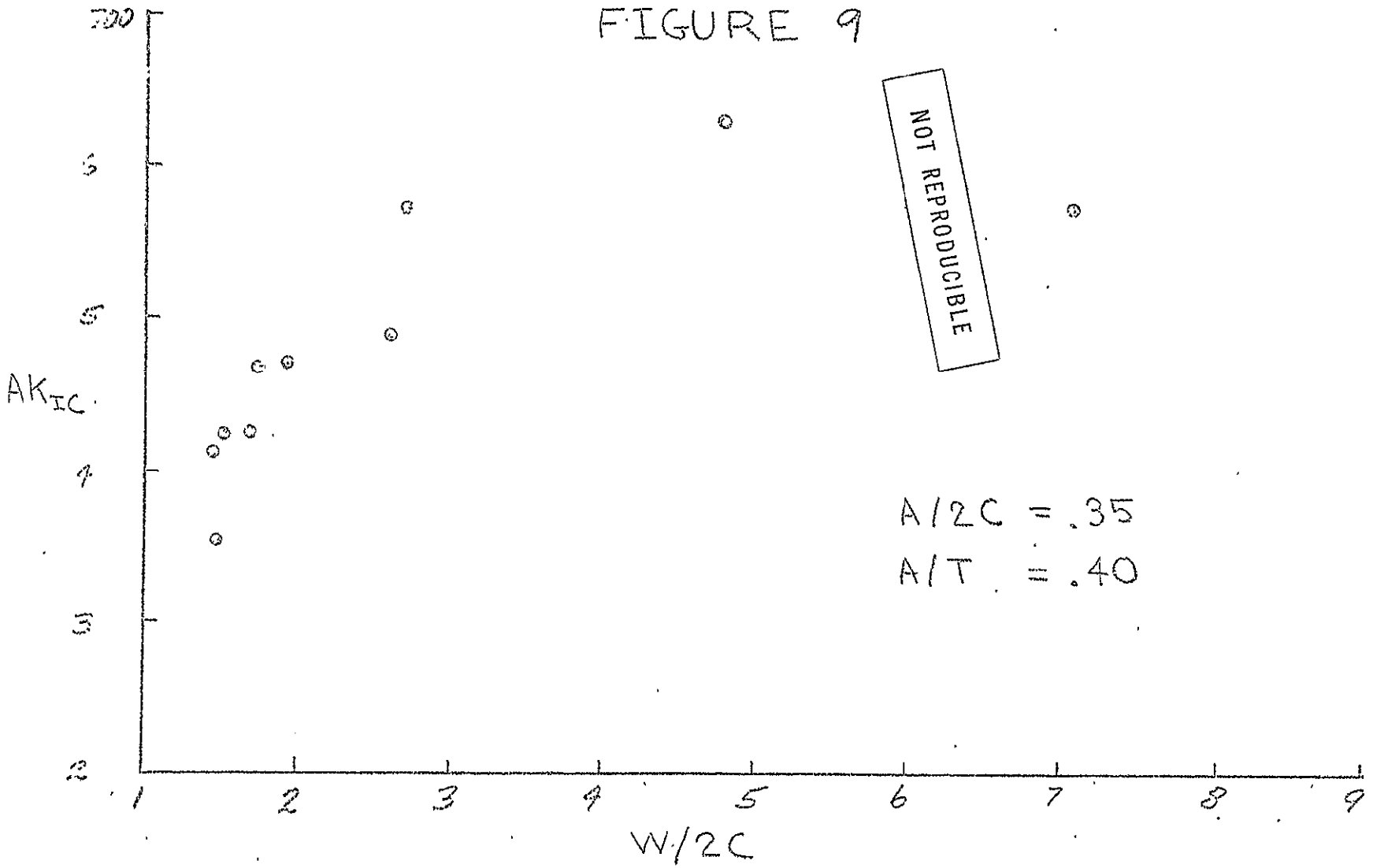

FIGURE 10

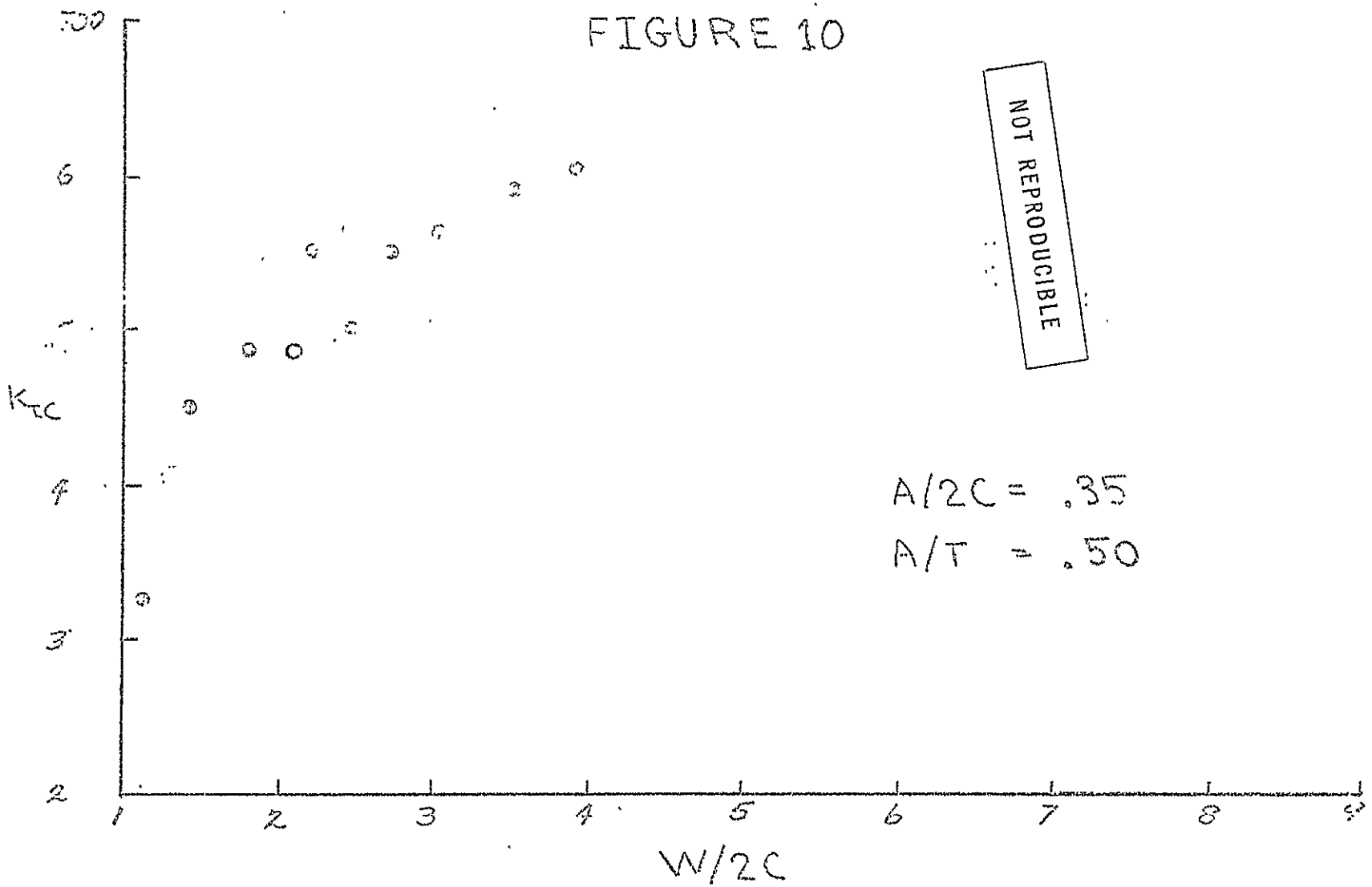

A/2C = .35

A/T = .50

FIGURE 11

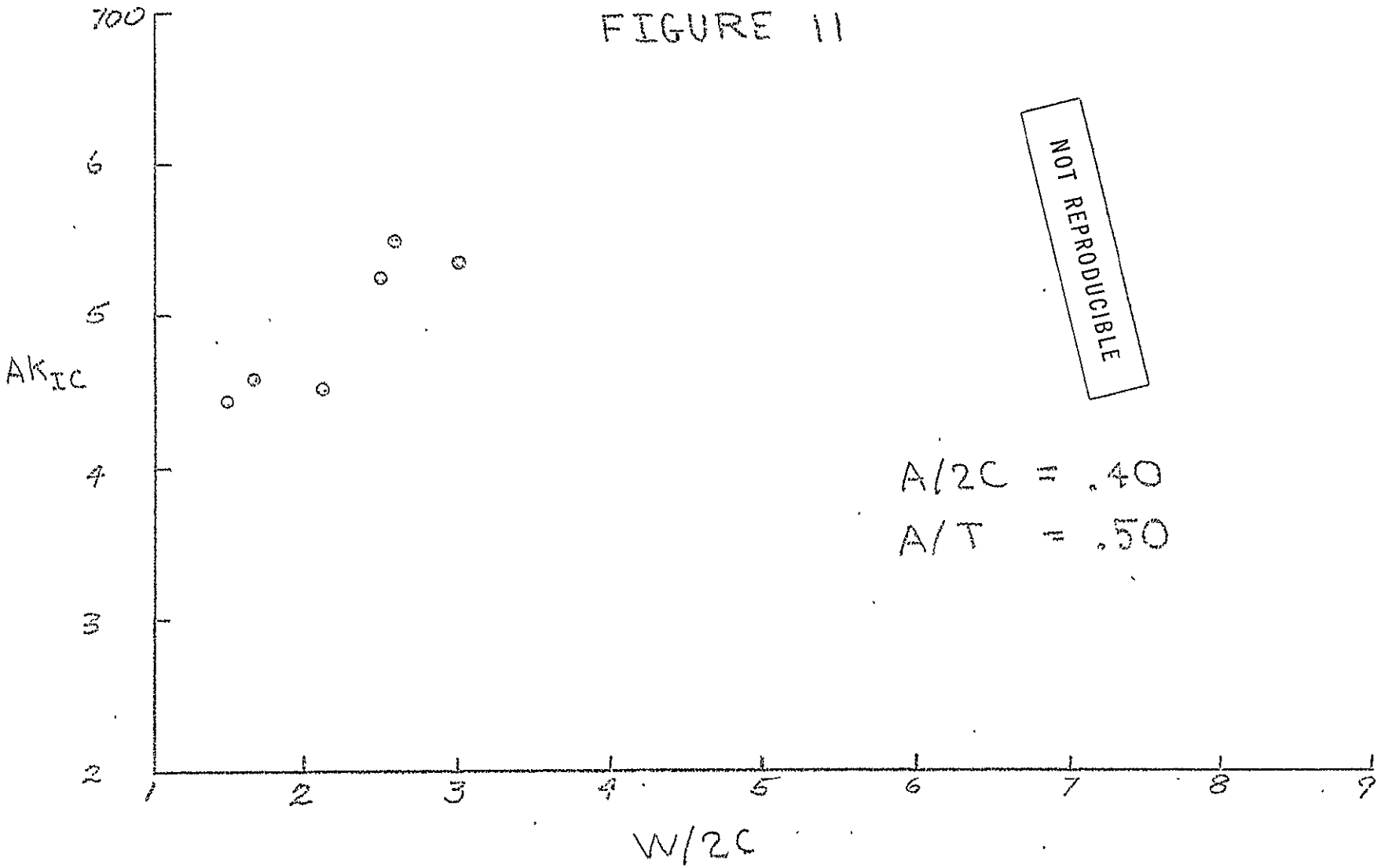

THESIS

A SURFACE CRACK IN A FINITE SOLID

Submitted by

Robert Wallace Thresher

In partial fulfillment of the requirements

for the Degree of Doctor of Philosophy

Colorado State University

Fort Collins, Colorado

August, 1970

COLORADO STATE UNIVERSITY

AUGUST, 1970

WE HEREBY RECOMMEND THAT THE THESIS PREPARED UNDER OUR SUPERVISION BY ROBERT WALLACE THRESHER ENTITLED A SURFACE CRACK IN A FINITE SOLID BE ACCEPTED AS FULFILLING IN PART REQUIREMENTS FOR THE DEGREE OF DOCTOR OF PHILOSOPHY.

Committee on Graduate Work

Adviser

H. G. Olson

Head of Department
Acting

ABSTRACT

A SURFACE CRACK IN A FINITE SOLID

A solution to the problem of a circular crack partially embedded in a solid of finite thickness is presented. A superposition and iteration technique is used to determine the stress intensity factor numerically. The stress intensity factor is determined as a function of position around the crack front for a variety of crack depths and thicknesses. The results of this study are compared to experimental data for a semi-elliptical surface flaw in a brittle material.

In addition, a solution for the partially closed Griffith crack is presented. This formulation leads to a closed form solution for the stress and displacement on the plane of the crack. A method for finding the open crack length is presented. The problem of pure bending which closes one end of the crack is solved and the stress intensity factor is calculated.

Robert Wallace Thresher
Department of Mechanical Engineering
Colorado State University
Fort Collins, Colorado 80521
August, 1970

ACKNOWLEDGEMENT

The author wishes to express his thanks to his advisor Dr. F. W. Smith, not only for his guidance and council in the preparation of this work, but for the many hours spent discussing interesting problems. The author is indebted to the Colorado State University computer center for providing a portion of the computer time necessary for this project.

This study was made possible through the financial support of the National Aeronautics and Space Administration under Grant No. NGR-06-002-063.

TABLE OF CONTENTS

LIST OF FIGURES

INTRODUCTION TO THE THESIS

The present form of fracture mechanics started with the work of Griffith in 1920 (1). The essence of Griffith's work stated that a crack will propagate if by doing so it can lower the total energy of the system. The stress analysis used by Griffith to calculate the stored elastic energy was taken from the work of Inglis (2) for an elliptic hole in the center of an infinite plate, where the minor axis of the ellipse was allowed to approach zero.

Another step toward the present theory of fracture mechanics was made when Irwin (3) pointed out that for metals the Griffith-type energy balance must be between the stored strain energy and the surface energy plus the work done during plastic deformation. Irwin also noted that for most engineering materials the work done against surface tension is small compared to the plastic work.

The Irwin-Griffith energy balance for a crack would appear as shown in Figure 1. As the crack size increases the stored elastic energy decreases and the amount of plastic work necessary to propagate the crack increases. However, the stored strain energy decreases at a faster rate and therefore creates an unstable situation when the crack is larger than a certain critical size.

In 1957 Irwin (4) showed that the strain energy release rate is related to the stress intensity factor K_I, where the stress intensity factor can be defined as

$$K_I = \lim_{\delta \to 0} \sqrt{2\pi\delta}\ \sigma_{xx}\Big|_{x=0}$$

for the situation illustrated in the bottom half of Figure 1. Since the strain energy release rate and the stress intensity factor are related, it is permissible to talk about a critical stress intensity factor. The critical stress intensity factor is the value of the stress intensity factor at which unstable crack propagation occurs. The critical stress intensity factor, which is called the fracture toughness, has been shown by experiment (5) to be a material property. The fracture mechanics failure criterion states that a crack will propagate if $K_I \geq K_{IC}$, where K_{IC} is the fracture toughness.

To determine whether a cracked component will fail in a given loading situation, one must have the fracture toughness for the material in question, and an elastic stress analysis from which to calculate K_I. For example, consider a two-dimensional crack of length $2a$ centered in a large plate loaded with a uniform tension σ. The plate is a brittle material which has a fracture toughness of 550 psi $\sqrt{in}$. A stress analysis is performed to obtain σ_{xx} on $x = 0$, from which the stress intensity factor is calculated. This computation gives

$$K_I = \sigma\sqrt{\pi a}$$

The fracture mechanics failure criterion states that this plate will fail when

$$\sigma\sqrt{\pi a} \geq 550$$

This equation gives the maximum allowable load σ for a given crack length $2a$. For most engineering materials the fracture toughness is

well documented. The difficult part of the problem is the stress analysis. Solutions to some of the more common problems can be found in the literature (5). However, many important problems are still unsolved. For example, surface cracks are very often seen in structural components, but only limited analysis has been performed on this type of crack.

The purpose of this thesis is to solve two problems in linear elastic fracture mechanics to obtain the stress intensity factor. Part I presents the solution for a surface flaw in a finite thickness plate. Part II presents the solution for a two dimensional through crack in which the applied load closes one end of the crack.

INTRODUCTION TO PART I

The three dimensional analysis of cracks started in 1945 with the work of Sneddon (6), who solved the problem of the circular crack in an infinite solid, where the crack was opened by a constant pressure. The corresponding problem for the elliptical crack in an infinite solid was done by Green and Sneddon in 1960 (7). More recently, Kassir and Sih (8, 9) solved the embedded elliptical crack for a prescribed shear, and later for a linearly varying normal pressure. The problems of an embedded hyperbola and an embedded parabola were solved by Shah (10). In addition, Shah solved the embedded elliptical crack for a normal pressure loading specified by a restricted polynomial (11).

Only limited analytical work has been done on surface crack problems. In 1962 Irwin (12) using the solution of Green and Sneddon estimated the stress intensity factor for a semi-elliptical crack in the surface of a half space. In 1965 Smith (13) solved the semi-circular crack in the surface of a half space, where the crack surface was loaded with an arbitrary normal pressure. In a continuation of Smith's work, Smith and Alavi solved the problem of a circular crack embedded in a half space (14) and the problem of the circular crack only partially embedded (15, 16).

The work contained herein is an extension and a refinement of the work of Smith and Alavi. It is the purpose of this portion of the thesis to present the solution to the part-circular crack in a finite

thickness solid. The work centers around determining stress intensity factors for circular flaws embedded an arbitrary depth into a plate of finite thickness.

CHAPTER I

THE SURFACE FLAW PROBLEM

1.1 The Problem Statement

Consider a circular crack embedded only part way into a plate as illustrated in Figure 2. The problem is to determine the stress intensity factor as a function of θ for a variety of depths D and A/T ratios under uniform tension loading.

Again referring to Figure 2, the boundary conditions may be stated as follows:

1. All normal and shearing stresses must vanish on both the front and back surfaces.
2. On the plane $z=0$:

   (a) $\sigma_{zz}\Big|_{z=0} = -P(r,\theta)$ inside the crack.

   (b) $U_z\Big|_{z=0} = 0$ outside the crack.

   (c) $\tau_{rz}\Big|_{z=0} = \tau_{\theta z}\Big|_{z=0} = 0$ all $z=0$.

The solution to this problem will be superimposed with a solution having a normal stress $+P(r,\theta)$ inside the crack to arrive at the boundary condition $\sigma_{zz}\Big|_{z=0} = 0$ inside the crack.

1.2 The Solution Method

The solution method which will be used is the Schwarz alternating technique (17). In this particular case the technique consists of using two elastic solutions coupled with an iteration procedure programmed for the digital computer to solve numerically for the stress intensity factor as a function of position along the crack border. The solutions used in this procedure are:

1. The circular crack in an infinite solid where the crack surface pressure is prescribed in the form of a Fourier series;
2. Stress in a half space due to pressure and shear on a rectangular portion of the half space boundary.

The iteration procedure works as follows:

1. The crack pressure, prescribed in the form of a Fourier series, is applied to the crack surface. For the case of simple tension, a constant pressure is applied to the crack surface. Solution 1 is used to calculate the resulting stress in the solid at the desired location for the front surface.
2. Stresses at the location of the front surface are removed using solution 2. This is accomplished by dividing the front surface into many small rectangles and applying "freeing" stresses to each rectangle which are equal and opposite to the stresses at the center of the rectangle as computed by solution 1. This freeing of the front surface produces a residual stress on the crack surface, which is computed using solution 2.

3. The negative of the stress residual on the crack surface is approximated with a Fourier series and this loading is then applied to free the crack surface of stress. Solution 1 is again used to compute the stress on the front surface.
4. Steps 2 and 3 are repeated until the residuals become negligible.

As the iteration continues, the stresses due to each step are also computed for the back surface and collected in a running sum. After convergence with the front surface has been obtained the iteration is done between the crack and the back surface, while a running total of residuals is kept on surface 1. This whole procedure is then repeated until residuals are negligible.

The elastic solution for the circular crack in an infinite solid will be developed in Chapter II and the solution for a rectangle on the surface of a half space will be discussed in Chapter III.

CHAPTER II

THE CIRCULAR CRACK IN AN INFINITE SOLID
SOLUTION 1

2.1 Boundary Conditions

Consider an elastic solid with a circular crack of radius "a" located on the plane $z=0$ which is opened by normal pressure $P(r,\theta)$. The crack and coordinate system are shown in Figure 3. The boundary conditions for this problem may be written as follows:

$$\text{(a)} \quad \sigma_{zz}\Big|_{z=0} = -P(r,\theta) \qquad \text{for} \quad 0 \leq r \leq a \qquad (2.1.1a)$$

$$\text{(b)} \quad U_z\Big|_{z=0} = 0 \qquad \text{for} \quad r > a \qquad (2.1.1b)$$

$$\text{(c)} \quad \tau_{rz}\Big|_{z=0} = \tau_{\theta z}\Big|_{z=0} = 0 \qquad (2.1.1c)$$

$$\text{(d)} \quad \sigma_{ij} \to 0 \quad \text{as} \quad x,y \to \infty \qquad (2.1.1d)$$

In addition, only normal crack pressures symmetric with the plane $z=0$ will be considered.

2.2 The Potential Formulation

The three dimensional form of the Navier equations can be written

$$G \nabla^2 U_i + (\lambda + G) U_{i,i} = 0 \qquad (2.2.1)$$

For the special class of problems where the shearing stresses are zero on the plane $z=0$ the following potential formulation satisfies the Navier equations:

$$U_r = \frac{\partial \phi}{\partial r} + (\beta^2 - 1) z \frac{\partial^2 \phi}{\partial r \partial z}$$

$$U_\theta = \frac{1}{r} \frac{\partial \phi}{\partial \theta} + (\beta^2 - 1) \frac{z}{r} \frac{\partial^2 \phi}{\partial \theta \partial z} \qquad (2.2.2)$$

$$U_z = - \beta^2 \frac{\partial \phi}{\partial z} + (\beta^2 - 1) z \frac{\partial^2 \phi}{\partial z^2}$$

where $\beta^2 = \frac{2(1 - \nu)}{(1 - 2\nu)}$

provided that $\nabla^2 \phi = 0$. This formation is presented by Green and Zerna (18).

Using Hooke's Law the stress components in terms of the potential function ϕ are easily found as

$$\sigma_{rr} = - 2(\beta^2-2) \frac{\partial^2 \phi}{\partial z^2} + 2 \frac{\partial^2 \phi}{\partial r^2} + 2(\beta^2-1) z \frac{\partial^3 \phi}{\partial r^2 \partial z}$$

$$\sigma_{\theta\theta} = - 2(\beta^2-2) \frac{\partial^2 \phi}{\partial z^2} + \frac{2}{r} \frac{\partial \phi}{\partial r} + \frac{2}{r^2} \frac{\partial^2 \phi}{\partial \theta^2}$$

$$+ 2(\beta^2-1) \frac{z}{r^2} \frac{\partial^3 \phi}{\partial \theta^2 \partial z} + 2(\beta^2-1) \frac{z}{r} \frac{\partial^2 \phi}{\partial r \partial z}$$

$$\sigma_{zz} = - 2(\beta^2-1) \frac{\partial^2 \phi}{\partial z^2} + 2(\beta^2-1) z \frac{\partial^3 \phi}{\partial z^3}$$

$$\tau_{r\theta} = \frac{2}{r}\frac{\partial^2\phi}{\partial r\partial\theta} + 2(\beta^2-1)\frac{z}{r}\frac{\partial^3\phi}{\partial\theta\partial z\partial r} - \frac{2}{r^2}\frac{\partial\phi}{\partial\theta}$$

$$- 2(\beta^2-1)\frac{z}{r^2}\frac{\partial^2\phi}{\partial\theta\partial z}$$

$$\tau_{rz} = 2(\beta^2-1)z\frac{\partial^3\phi}{\partial r\partial z^2}$$

$$\tau_{\theta z} = 2(\beta^2-1)\frac{z}{r}\frac{\partial^3\phi}{\partial\theta\partial z^2} \qquad (2.2.3)$$

The displacements in (2.2.2) have been nondimensionalized through division by "a", the crack radius. The stress has been nondimensionalized with respect to the shear modulus.

From the form of the potential formulation it can be seen that the boundary condition (2.1.1c) is automatically satisfied while boundary conditions (2.1.1a) and (2.1.1b) on the plane $z=0$ reduce to

$$\frac{\partial^2\phi}{\partial z^2} = \frac{P(r,\theta)}{2(\beta^2 - 1)} \qquad \text{for } 0 \le r \le a \qquad (2.2.4a)$$

$$\frac{\partial\phi}{\partial z} = 0 \qquad \text{for } r > 0 \qquad (2.2.4b)$$

2.3 The Potential Function

To satisfy the mixed boundary conditions of (2.2.4a) and (2.2.4b) the potential function, ϕ, will be assumed in the form

$$\phi = \sum_{n=0}^{N} \cos(n\theta) \int_0^\infty \frac{f_n(\xi)}{\xi} J_n(\xi r)\, e^{-z\xi}\, d\xi \qquad (2.3.1)$$

This potential function clearly satisfies the boundary condition (2.1.1d), since both $J_n(\xi r)$ and $e^{-z\xi}$ tend toward zero for large r and z. The remaining boundary conditions to be satisfied are (2.2.4a) and (2.2.4b), which after substitution for ϕ may be rewritten as

$$\frac{P(r,\theta)}{2(\beta^2-1)} = \sum_{n=0}^{N} \cos(n\theta) \int_0^\infty \xi f_n(\xi) J_n(\xi r)\, d\xi \qquad (2.2.3a)$$

for $r \leq 1$

$$0 = \sum_{n=0}^{N} \cos(n\theta) \int_0^\infty f_n(\xi) J_n(\xi r)\, d\xi \qquad (2.3.2b)$$

for $r > 1$

To find the unknown function $f_n(\xi)$, the function $P(r,\theta)/2(\beta^2-1)$ will be expanded in a Fourier cosine series as follows:

$$\frac{P(r,\theta)}{2(\beta^2-1)} = \sum_{n=0}^{N} B_n(r) \cos(n\theta) \qquad (2.3.3)$$

where the Fourier coefficients $B_n(r)$ are given by

$$B_0(r) = \frac{1}{2\pi(\beta^2-1)} \int_0^\pi P(r,\theta)\, d\theta$$

and (2.3.4)

$$B_n(r) = \frac{1}{\pi(\beta^2-1)} \int_0^\pi P(r,\theta) \cos(n\theta)\, d\theta$$

Now the boundary conditions (2.3.2a) and (2.3.2b) may be further simplified to give the following set of dual integral equations:

$$B_n(r) = \int_0^\infty \xi f_n(\xi)\, J_n(\xi r)\, d\xi \qquad \text{for } 0 \le r \le 1 \tag{2.3.5a}$$

$$0 = \int_0^\infty f_n(\xi)\, J_n(\xi r)\, d\xi \qquad \text{for } r > 1 \tag{2.3.5b}$$

The solution to these dual integral equations for the unknown function $f_n(\xi)$, due to Busbridge, is given by Sneddon in (19) as

$$f_n(\xi) = \sqrt{\frac{2\xi}{\pi}} \int_0^1 \eta^{3/2}\, J_{n+\frac{1}{2}}(\xi\eta)\, d\eta \int_0^1 B_n(\eta\rho)\, \frac{\rho^{n+1}}{\sqrt{1-\rho^2}}\, d\rho \tag{2.3.6}$$

2.4 The Function $f_n(\xi)$

In order to reduce the complexity of the integrations required to determine $f_n(\xi)$, the function $B_n(r)$ will be expanded in the power series

$$B_n(r) = \sum_{p=0}^{P} C_n^{\,p}\, r^p \tag{2.4.1}$$

where $C_n^{\,p}$ = constant. Substitution of this representation for $B_n(r)$ into (2.3.6) and performing the integration on ρ gives

$$f_n(\xi) = \frac{1}{\sqrt{2}} \sum_{p=0}^{P} C_n^{\,p}\, H_n^{\,p}\, \xi^{\frac{1}{2}} \int_0^1 \eta^{p+3/2}\, J_{n+\frac{1}{2}}(\xi\eta)\, d\eta \tag{2.4.2}$$

where

$$H_n^{\,p} = \frac{\Gamma\left[\frac{p+n+2}{2}\right]}{\Gamma\left[\frac{p+n+3}{2}\right]} \tag{2.4.3}$$

To this point the solution development has followed the work of Smith and Alavi (15), who expanded the Bessel function $J_{n+\frac{1}{2}}(\xi\eta)$ in a power series which was then integrated term by term and substituted into the potential function ϕ to obtain a series solution for the stress components. Because the series solution did not converge for $r^2 + z^2 \leq 1$, they were forced to develop a closed form solution for small r and z. The main drawback with the closed form solution was that it required a considerable amount of hand computation to complete the required integrations. Even then it took a significant amount of computer time to calculate numerical values for the stresses. As a result of these difficulties, Alavi's solution is limited to three terms in both the Fourier series (2.3.3) and the power series (2.4.1). In order to extend the solution to include more terms in the Fourier series and power series, a numerical integration scheme was devised.

Watson (20) gives the integral representation for $J_{n+\frac{1}{2}}(\xi\eta)$ as

$$J_{n+\frac{1}{2}}(\xi\eta) = \frac{(\frac{1}{2}\xi\eta)^{n+\frac{1}{2}}}{\Gamma(n+1)\sqrt{\pi}} \int_{-1}^{1} (1-t^2)^n \, e^{i\xi\eta t} \, dt \qquad (2.4.4)$$

Substitution of this integral representation into equation (2.4.2), and then substitution of equation (2.4.2) into equation (2.3.1) gives the result

$$\phi = \sum_{n=0}^{N} \frac{\cos(n\theta)}{\pi 2^{n+1} \Gamma(n+1)} \sum_{p=0}^{P} C_n^p H_n^p \times$$

$$\int_0^1 \int_{-1}^{1} \eta^{p+n+2} (1-t^2)^n \, dt \, d\eta \int_0^{\infty} \xi^n J_n(\xi r) e^{-\xi(z-i\eta t)} \, d\xi \qquad (2.4.5)$$

The last integral in (2.4.5) has the value

$$\int_0^\infty \xi^n J_n(\xi r) e^{-\xi(z-i\eta t)} d\xi = \frac{\Gamma(2n+1) r^n}{2^n \Gamma(n+1) [(z-i\eta t)^2+r^2]^{(2n+1)/2}} \tag{2.4.6}$$

Substitution of equation (2.4.6) into equation (2.4.5) gives

$$\phi = \sum_{n=0}^{N} \frac{\cos(n\theta)\, \Gamma(2n+1)}{\sqrt{\pi}\, 2^{2n+1} [\Gamma(n+1)]^2} \sum_{p=0}^{P} C_n^p H_n^p r^n I(n,p) \tag{2.4.7}$$

where

$$I(n,p) = \int_0^1 \int_{-1}^1 \frac{\eta^{p+n+2} (1-t^2)^n}{[(z-i\eta t)^2+r^2]^{(2n+1)/2}} \, dt d\eta \tag{2.4.8}$$

2.5 The Stress Components

To determine the stress components, the equation (2.4.8) for I(n,p) must be substituted into the equations (2.2.3), which gives the following integrals to be evaluated:

$$FI(1) = \int_0^1 \int_{-1}^1 \frac{W}{Q^{(2n+1)/2}} \, dt d\eta \tag{2.5.1}$$

$$FI(2) = \int_0^1 \int_{-1}^1 \frac{W}{Q^{(2n+3)/2}} \, dt d\eta \tag{2.5.2}$$

$$FI(3) = \int_0^1 \int_{-1}^1 \frac{W}{Q^{(2n+5)/2}} \, dt d\eta \tag{2.5.3}$$

$$FI(4) = \int_0^1 \int_{-1}^1 \frac{W(z-i\eta t)}{Q^{(2n+3)/2}}\, dt d\eta \qquad (2.5.4)$$

$$FI(5) = \int_0^1 \int_{-1}^1 \frac{W(z-i\eta t)}{Q^{(2n+5)/2}}\, dt d\eta \qquad (2.5.5)$$

$$FI(6) = \int_0^1 \int_{-1}^1 \frac{W(z-i\eta t)}{Q^{(2n+7)/2}}\, dt d\eta \qquad (2.5.6)$$

$$FI(7) = \int_0^1 \int_{-1}^1 \frac{W(z-i\eta t)^2}{Q^{(2n+5)/2}}\, dt d\eta \qquad (2.5.7)$$

$$FI(8) = \int_0^1 \int_{-1}^1 \frac{W(z-i\eta t)^2}{Q^{(2n+7)/2}}\, dt d\eta \qquad (2.5.8)$$

where

$$W = \eta^{p+n+2}(1-t^2)^n$$

and

$$Q = [(z-i\eta t)^2 + r^2]$$

A computer program was written to integrate the FI(1) through FI(8) integrals numerically whenever they occur. The integration formula used was a 12th order Newton-Cotes closed type formula (21). Even with this high order formula, a very fine mesh was required for small z and $r < 1$. In addition, the integration accuracy deteriorates with increasing n. However, despite these problems the integrals could be calculated to 3 digit accuracy for z as low as .2 for $r < 1$, and for n and p as high as 5. The only drawback in going to smaller

z and larger n , is that the required computer time tends to increase very rapidly. No integration problems were encountered when $r > 1$, even for $z=0$. The stress components may be written as follows:

$$\sigma_{rr} = \sum_{n=0}^{N} A(n) \cos(n\theta) \sum_{p=0}^{P} C_n^p H_n^p r^n \, SRR \qquad (2.5.9)$$

$$\sigma_{\theta\theta} = \sum_{n=0}^{N} A(n) \cos(n\theta) \sum_{p=0}^{P} C_n^p H_n^p r^n \, S\theta\theta \qquad (2.5.10)$$

$$\tau_{r\theta} = -\sum_{n=0}^{N} A(n) \sin(n\theta) \sum_{p=0}^{P} C_n^p H_n^p r^n \, SR\theta \qquad (2.5.11)$$

$$\tau_{rz} = \sum_{n=0}^{N} A(n) \cos(n\theta) \sum_{p=0}^{P} C_n^p H_n^p r^n \, SRZ \qquad (2.5.12)$$

$$\tau_{\theta z} = -\sum_{n=0}^{N} A(n) \sin(n\theta) \sum_{p=0}^{P} C_n^p H_n^p r^n \, S\theta Z \qquad (2.5.13)$$

where

$$\begin{aligned} SRR = &- C1 \cdot FI(7) + C14 \cdot FI(2) + C2 \cdot FI(1) \\ &- C3 \cdot FI(1) + C4 \cdot FI(3) - C5 \cdot FI(4) \\ &+ C6 \cdot FI(5) + C7 \cdot FI(6) \end{aligned} \qquad (2.5.14)$$

$$\begin{aligned} S\theta\theta = &- C1 \cdot FI(7) + C14 \cdot FI(2) - C2 \cdot FI(1) \\ &- C8 \cdot FI(2) + C5 \cdot FI(4) + C9 \cdot FI(5) \end{aligned} \qquad (2.5.15)$$

$$\begin{aligned} SR\theta = &\; C2 \cdot FI(1) - C10 \cdot FI(2) - C5 \cdot FI(4) \\ &+ C11 \cdot FI(5) \end{aligned} \qquad (2.5.16)$$

$$\begin{aligned} SRZ = &\; C12 \cdot FI(7) - C13 \cdot FI(8) - C15 \cdot FI(2) \\ &+ C16 \cdot FI(3) \end{aligned} \qquad (2.5.17)$$

$$S\theta Z = C12 \cdot FI(7) - C15 \cdot FI(2) \qquad (2.5.18)$$

and

$$A(n) = \frac{\Gamma(2n+1)}{\sqrt{\pi}\, 2^{2n+1} [\Gamma(n+1)]^2}$$

$$C1 = 2(\beta^2-2)(2n+3)(2n+1)$$

$$C2 = 2n(n-1)/r^2$$

$$C3 = 2(2n+1)^2$$

$$C4 = 2(2n+1)(2n+3)r^2$$

$$C5 = 2(\beta^2-1)zn(n-1)(2n+1)/r^2$$

$$C6 = 2(\beta^2-1)z(2n+1)^2(2n+3)$$

$$C7 = 2(\beta^2-1)z(2n+1)(2n+3)(2n+5)r^2$$

$$C8 = 2(2n+1)$$

$$C9 = 2(\beta^2-1)z(2n+1)(2n+3)$$

$$C10 = 2n(2n+1)$$

$$C11 = 2(\beta^2-1)zn(2n+1)(2n+3)$$

$$C12 = 2(\beta^2-1)zn(2n+1)(2n+3)/r$$

$$C13 = 2(\beta^2-1)z(2n+1)(2n+3)(2n+5)r$$

$$C14 = 2(\beta^2-2)(2n+1)$$

$$C15 = 2(\beta^2-1)zn(2n+1)/r$$

$$C16 = 2(\beta^2-1)z(2n+1)(2n+3)r$$

The equations (2.5.9) through (2.5.13) together with the integrals given in equations (2.5.1) through (2.5.8) give the stresses near a circular crack in an infinite solid. Due to the problems with the numerical integration procedure for small z the special solution for $z=0$ and $r < 1$ will be presented in the next section.

2.6 The Solution for $z=0$ and $r < 1$

The stress components for the special case $z=0$ have the form

$$\sigma_{rr}\Big|_{z=0} = -2(\beta^2-2)\frac{\partial^2\phi}{\partial z^2} + 2\frac{\partial^2\phi}{\partial r^2} \qquad (2.6.1)$$

$$\sigma_{\theta\theta}\Big|_{z=0} = -2(\beta^2-2)\frac{\partial^2\phi}{\partial z^2} + \frac{2}{r}\frac{\partial\phi}{\partial r} + \frac{2}{r^2}\frac{\partial^2\phi}{\partial\theta^2} \qquad (2.6.2)$$

$$\tau_{r\theta}\Big|_{z=0} = \frac{2}{r}\frac{\partial^2\phi}{\partial r\partial\theta} - \frac{2}{r^2}\frac{\partial\phi}{\partial\theta} \qquad (2.6.3)$$

The potential function itself becomes

$$\phi\Big|_{z=0} = \sum_{n=0}^{N}\frac{\cos(n\theta)}{\sqrt{2}}\sum_{p=0}^{P} C_n^p H_n^p \int_0^1 \eta^{p+3/2}\, d\eta \times$$

$$\int_0^\infty J_{n+\frac{1}{2}}(\xi\eta)\, J_n(\xi r)\frac{d\xi}{\sqrt{\xi}} \qquad (2.6.4)$$

while $\dfrac{\partial^2\phi}{\partial z^2}\Big|_{z=0}$ is given by

$$\left.\frac{\partial^2\phi}{\partial z^2}\right|_{z=0} = \sum_{n=0}^{N} \frac{\cos(n\theta)}{\sqrt{2}} \sum_{p=0}^{P} C_n^p H_n^p \int_0^1 \eta^{p+3/2}\, d\eta \times$$

$$\int_0^\infty \xi^{3/2} J_{n+\frac{1}{2}}(\xi\eta)\, J_n(\xi r)\, d\xi \qquad (2.6.5)$$

To determine the stresses on the plane $z=0$, the integrals involved in these two expressions must be evaluated.

The infinite integral in equation (2.6.4) is a Weber-Schafheitlin discontinuous integral. Abramowitz and Stegun (21) give the value for this integral as

$$\int_0^\infty \frac{J_\mu(at)\, J_\nu(bt)}{t^\lambda}\, dt =$$

$$\frac{b^\nu\, \Gamma\left[\frac{\mu+\nu-\lambda+1}{2}\right]}{2^\lambda\, a^{\nu-\lambda+1}\, \Gamma(\nu+1)\, \Gamma\left[\frac{\mu-\nu+\lambda+1}{2}\right]}\; {}_2F_1\left[\frac{\mu+\nu-\lambda+1}{2}, \frac{\mu-\nu-\lambda+1}{2}; \nu+1; \frac{b^2}{a^2}\right]$$

for $0 < b < a$, $\lambda > -1$ and $(\mu+\nu-\lambda+1) > 0$, or

$$\frac{a^\mu\, \Gamma\left[\frac{\mu+\nu-\lambda+1}{2}\right]}{2^\lambda\, b^{\mu-\lambda+1}\, \Gamma(\mu+1)\, \Gamma\left[\frac{\nu-\mu+\lambda+1}{2}\right]}\; {}_2F_1\left[\frac{\mu+\nu-\lambda+1}{2}, \frac{\mu-\nu-\lambda+1}{2}; \mu+1; \frac{a^2}{b^2}\right]$$

for $0 < a < b$, $\lambda > -1$ and $(\mu+\nu-\lambda+1) > 0$

where the function ${}_2F_1(a,b;c;z)$ is the Gauss hypergeometric series (21).

The infinite integral of (2.6.4) becomes

$$\int_0^\infty J_{n+\frac{1}{2}}(\xi\eta)\, J_n(\xi r)\, \frac{d\xi}{\sqrt{\xi}} =$$

$$\frac{r^n\, \Gamma(n+\frac{1}{2})}{\sqrt{2}\, \eta^{n+\frac{1}{2}}\, \Gamma(n+1)} \quad , \text{ for } \quad 0 < r < \eta \ , \text{ and}$$

$$\frac{\eta^{n+\frac{1}{2}}}{\sqrt{2}\, r^{n+1}\, \pi} \sum_{s=0}^{\infty} \frac{\Gamma(n+s+\frac{1}{2})\Gamma(s+\frac{1}{2})}{\Gamma(n+s+3/2)\, s!} \left[\frac{\eta^2}{r^2}\right]^s \quad \text{for} \quad 0 < \eta < r \ . \tag{2.6.6}$$

Substitution of equation (2.6.6) into equation (2.6.4) gives

$$\phi\Big|_{z=0} = \sum_{n=0}^{N} \frac{\cos(n\theta)}{\sqrt{2}} \sum_{p=0}^{P} C_n^p\, H_n^p \times$$

$$\left\{ \int_0^r \eta^{p+3/2} \left\{ \frac{\eta^{n+\frac{1}{2}}}{\sqrt{2}\, r^{n+1}\, \pi} \sum_{s=0}^{\infty} \frac{\Gamma(n+s+\frac{1}{2})\Gamma(s+\frac{1}{2})}{\Gamma(n+s+3/2)\, s!} \left[\frac{\eta}{r}\right]^{2s} \right\} d\eta \right.$$

$$\left. + \int_r^1 \eta^{p+3/2} \left[\frac{r^n\, \Gamma(n+\frac{1}{2})}{\sqrt{2}\, \eta^{n+\frac{1}{2}}\, \Gamma(n+1)} \right] d\eta \right\} \tag{2.6.7}$$

Interchanging the integration and the summation in equation (2.6.7) and proceeding to evaluate the next integral gives

$$\phi\Big|_{z=0} = \sum_{n=0}^{N} \frac{\cos(n\theta)}{\sqrt{2}} \sum_{p=0}^{P} C_n^p\, H_n^p \left\{ r^{p+2}\, BT(n,p) \right.$$

$$\left. + \frac{\Gamma(n+\frac{1}{2})}{\Gamma(n+1)} \begin{cases} \dfrac{1}{(p-n+2)} (r^n - r^{p+2}) & \text{for} \quad p-n+1 \neq -1 \\ -\, r^n \log(r) & \text{for} \quad p-n+1 = -1 \end{cases} \right\} \tag{2.6.8}$$

where

$$BT(n,p) = \sum_{s=0}^{\infty} \frac{\Gamma(n+s+\frac{1}{2})\ \Gamma(s+\frac{1}{2})}{\Gamma(n+s+3_2)\Gamma(s+1)(n+p+2s+3)} \qquad (2.6.9)$$

Equation (2.6.8) together with (2.6.9) give the value of ϕ on the plane $z=0$.

To find $\partial^2\phi/\partial z^2\big|_{z=0}$, the integrals in equation (2.6.5) must be evaluated. A careful examination of the infinite integral in equation (2.6.5) shows that it does not exist. However, the form of the infinite integral can be changed by integrating the finite integral on η by parts. The basic differentiation formula for Bessel functions can be used to show that

$$\frac{d}{d\eta}\left\{\frac{\eta^{-n+\frac{1}{2}}}{\xi} J_{n-\frac{1}{2}}(\xi\eta)\right\} = \eta^{-n+\frac{1}{2}} J_{n+\frac{1}{2}}(\xi\eta) \qquad (2.6.10)$$

The integral on η can be rewritten to give

$$\int_0^1 \eta^{p+3/2} J_{n+\frac{1}{2}}(\xi\eta)d\eta = -\int_0^1 (\eta^{p+n+1}) \times$$

$$[-\eta^{-n+\frac{1}{2}} J_{n+\frac{1}{2}}(\xi\eta)d\eta\ ] \qquad (2.6.11)$$

Integrating (2.6.11) by parts gives

$$\int_0^1 \eta^{p+3/2} J_{n+\frac{1}{2}}(\xi\eta)d\eta =$$

$$-\frac{J_{n-\frac{1}{2}}(\xi)}{\xi} + (p+n+1)\int_0^1 \frac{\eta^{p+\frac{1}{2}}}{\xi} J_{n-\frac{1}{2}}(\xi\eta)d\eta \qquad (2.6.12)$$

Substitution of equation (2.6.12) into the expression (2.6.5) gives

$$\left.\frac{\partial^2\phi}{\partial z^2}\right|_{z=0} = \sum_{n=0}^{N} \frac{\cos(n\theta)}{\sqrt{2}} \sum_{p=0}^{P} C_n^p H_n^p \times$$

$$\left\{(p+n+1) \int_0^1 \eta^{p+\frac{1}{2}} d\eta \int_0^\infty \sqrt{\xi}\, J_{n-\frac{1}{2}}(\xi\eta)\, J_n(\xi r) d\xi \right.$$

$$\left. \int_0^\infty \sqrt{\xi}\, J_{n-\frac{1}{2}}(\xi)\, J_n(\xi r) d\xi \right\} \qquad (2.6.13)$$

As was expected, these integrals are also special cases of the Weber-Schafheitlin discontinuous integral and can be evaluated to give

$$\int_0^\infty \sqrt{\xi}\, J_{n-\frac{1}{2}}(\xi)\, J_n(r\xi) d\xi = 0 \qquad \text{for } 0 < r < 1 \qquad (2.6.14)$$

$$\int_0^\infty \sqrt{\xi}\, J_{n-\frac{1}{2}}(\xi\eta)\, J_n(r\xi) d\xi = 0 \qquad \text{for } 0 < r < \eta \qquad (2.6.15)$$

$$\int_0^\infty \sqrt{\xi}\, J_{n-\frac{1}{2}}(\xi\eta)\, J_n(r\xi) d\xi = \frac{\sqrt{2}\, \eta^{n-\frac{1}{2}} (r^2-\eta^2)^{-\frac{1}{2}}}{r^n \sqrt{\pi}} \qquad \text{for } r > \eta > 0 . \qquad (2.6.16)$$

Because the solution developed in 2.5 is perfectly acceptable for $z=0$ and $r > 1$, the solution in this section will be developed only for the case $r < 1$. With this restriction, $\left.\partial^2\phi/\partial z^2\right|_{z=0}$ may be written as

$$\left.\frac{\partial^2\phi}{\partial z^2}\right|_{z=0} = \sum_{n=0}^{N} \frac{\cos(n\theta)}{\sqrt{2}} \sum_{p=0}^{P} C_n^p H_n^p \times$$

$$\frac{(p+n+1)}{r^n \sqrt{\pi}} \int_0^r \frac{\eta^{p+n}}{(r^2-\eta^2)^{\frac{1}{2}}}\, d\eta \qquad \text{for } r < 1 \ . \tag{2.6.17}$$

After performing the final integration, $\left.\partial^2\phi/\partial z^2\right|_{z=0}$ takes the form

$$\left.\frac{\partial^2\phi}{\partial z^2}\right|_{z=0} = \sum_{n=0}^{N} \frac{\cos(n\theta)}{2} \sum_{p=0}^{P} (p+n+1)\, C_n^p H_n^p \times$$

$$\begin{cases} \sqrt{\pi} & \text{for } n+p = 0 \\ \dfrac{\Gamma\left[\frac{n+p+2}{2}\right]}{\Gamma\left[\frac{n+p+3}{2}\right]} r^p & \text{for } n+p \neq 0 \end{cases} \quad \text{for } r < 1 \ . \tag{2.6.18}$$

The stress components for the plane $z=0$ can be calculated by substituting the equations (2.6.8) and (2.6.18) into the equations (2.6.1) through (2.6.3).

$$\left.\sigma_{rr}\right|_{z=0} = \sum_{n=0}^{N} \frac{\cos(n\theta)}{\pi} \sum_{p=0}^{P} C_n^p H_n^p r^p \times$$

$$\left\{ BT(n,p)(p+2)(p+1) - (\beta^2-2)\pi \begin{cases} \sqrt{\pi} & \text{for } n+p = 0 \\ H_n^p & \text{for } n+p \neq 0 \end{cases} \right.$$

$$\left. + \begin{cases} \frac{1}{2}\pi\,\Gamma(n+\frac{1}{2}) \\ \overline{\Gamma(n+1)(p-n+2)} \end{cases} [n(n-1)r^{n-p-2} - (p+2)(p+1)] \quad \text{for } p-n+1 \neq -1 \right.$$

$$\left. \begin{cases} -\dfrac{\pi\,\Gamma(n+\frac{1}{2})}{\Gamma(n+1)} r^{n-p-2} [n(n-1)\log(r) + 2n - 1] & \text{for } p-n+1 = -1 \end{cases} \right\} \tag{2.6.19}$$

$$\sigma_{\theta\theta}\Big|_{z=0} = \sum_{n=0}^{N} \frac{\cos(n\theta)}{\pi} \sum_{p=0}^{P} C_n^p H_n^p r^p \times$$

$$\left\{ (p-n^2+2)\, BT(n,p) - (\beta^2-1)\pi \begin{cases} \sqrt{\pi} & \text{for } n+p = 0 \\ H_n^p & \text{for } n+p \neq 0 \end{cases} \right\}$$

$$+ \left\{ \begin{cases} \frac{\pi\,\Gamma(n+\frac{1}{2})}{\Gamma(n+1)(p-n+2)} \left[n(1-n) r^{n-p-2} + n^2-p-2 \right] & \text{for } p-n+1 \neq -1 \\ -\frac{\pi\,\Gamma(n+\frac{1}{2})}{\Gamma(n+1)} r^{n-p-2} \left[n(1-n)\log(r) + 1 \right] & \text{for } p-n+1 = -1 \end{cases} \right\} \quad (2.6.20)$$

$$\tau_{r\theta}\Big|_{z=0} = \sum_{n=0}^{N} \frac{\sin(n\theta)}{\pi} \sum_{p=0}^{P} C_n^p H_n^p r^p \left\{ -n(p+1)\, BT(n,p) \right.$$

$$\left. + \left\{ \begin{cases} -\frac{\pi\,\Gamma(n+\frac{1}{2})\, n}{\Gamma(n+1)(p-n+2)} \left[(n-1) r^{n-p-2} - p-1 \right] & \text{for } p-n+1 \neq -1 \\ \frac{\pi\,\Gamma(n+\frac{1}{2})}{\Gamma(n+1)} n(n-1)\left[\log(r) + 1 \right] & \text{for } p-n+1 = -1 \end{cases} \right\} \right\} \quad (2.6.21)$$

$$\tau_{rz}\Big|_{z=0} = \tau_{z\theta}\Big|_{z=0} = 0 \quad (2.6.22)$$

Equations (2.5.9) through (2.5.13) together with equations (2.6.19) through (2.6.22) constitute the complete circular crack solution.

2.7 The Stress Intensity Factor

The stress intensity factor K_I is defined by

$$K_I = \lim_{\delta \to 0} \sqrt{2\pi\delta}\ \sigma_{zz}\Big|_{z=0} \tag{2.7.1}$$

where δ is the distance from the crack tip and σ_{zz} is the normal stress on the plane of the crack. Substitution of σ_{zz} into equation (2.7.1) yields

$$K_I = 2G(\beta^2-1) \sum_{n=0}^{N} \cos(n\theta) \sum_{p=0}^{P} C_n^p H_n^p \tag{2.7.2}$$

This method of calculating K_I was first used by Smith (13).

2.8 Summary

In Chapter II the problem of the circular crack in an infinite solid has been formulated and solved. Section 2.5 presents the stress components in the form of a double series. Some of the required integrations must be performed numerically and these are given in equations (2.5.1) through (2.5.8). Section 2.6 presents the stress components for the special case $z=0$ and $r < 1$. This special case had to be solved separately because of problems with the numerical integration procedure for small z. Section 2.7 presents a method for determining the stress intensity factor for an arbitrary normal pressure on the crack surface.

The solution presented in this chapter can be used to calculate the stresses surrounding a circular crack in an infinite solid, when the crack surface is loaded with a normal pressure approximated by a

truncated Fourier-power series. The Fourier series contains terms up to $\cos(5\theta)$, while the power series includes terms up to r^4. In addition, a direct method of calculating the stress intensity factor due to this loading has been presented.

CHAPTER III

THE HALF SPACE SOLUTION

SOLUTION 2

3.1 The General Problem

In section 2.2 it was explained that solution 2 would be used to calculate the stress on the crack surface produced by freeing of the front and back surfaces during the iteration procedure. Figure 4 is an illustration of how the front and back surfaces are arranged for this procedure. The following paragraphs describe how this portion of the procedure functions.

After the stresses at the center of each rectangle have been computed using solution 1, solution 2 is used to calculate the stress on the crack surface produced by the freeing process. To accomplish this the crack surface is represented as a circular array of points and the stress at each of the array points is calculated by summing the stresses produced by each individual rectangle of the front surface.

The freeing stress which produces a stress σ_{zz} on the crack surface also produces stresses on the back surface. This is handled by considering each back surface rectangle one at a time and summing the stresses produced by freeing each of the front surface rectangles. Here again, the stress calculation is made for the center of each rectangle. The calculations proceed in an identical manner for iteration between the back surface and the crack.

To save computer time, the stress calculations between the front and back surfaces are made only after an iteration cycle between the crack and one surface has been completed. For example, if three iterations are to be performed between the front surface and the crack then the freeing stresses for each iteration are accumulated in a running sum and the back surface residual stress is calculated only once.

3.2 The Solution for One Rectangle

For any given rectangle the problem reduces to finding a solution for a semi-infinite solid when the rectangle on the boundary is subjected to uniform normal and shearing stresses. This basic problem has a rather long history and was once called the "problem of Boussinesq and Cerruti." A potential formulation for the problem is presented in Love's "A Treatise on the Mathematical Theory of Elasticity" (22). Later, in a paper (23) Love presents the solution for the case of constant normal stress. Much more recently Smith and Alavi presented the solution for the case of constant shearing stresses. Since the solution is rather involved and adds little to the understanding of this work, the solution will not be reproduced here. For a more complete discussion of this solution and its application to similar problems in fracture mechanics see references (13) (14) and (15). The formulas given by Love (23), and by Smith and Alavi (15) were programed for the digital computer so that wherever the freeing process was required these subroutines could be used.

CHAPTER IV

THE COMPUTER PROGRAM

4.1 The Program Logic

This section gives a description of how the computer was programmed to use the two elastic solutions to solve the surface flaw problem. The essence of the material which will be given here was previously presented in section 2.2. However, at that point it was intended as an introduction to the solution method rather than a description of how the solution was obtained.

A block diagram of the computer program is shown in Figure 5. The number to the right of a block is the statement number in the main program where that block operation takes place. Although the block diagram does not give all of the details of the program operation, it does present the basic program logic.

4.2 Program Checkout

To insure that the program had no computational errors, a variety of test cases were run. For example, the circular crack solution was checked by comparing the results of this program with the closed form solution of Sneddon for the special case of a constant crack pressure. In addition, the program was checked against Alavi's solution for a crack pressure described by three terms in the Fourier series. In both cases the comparison was accurate to at least three digits.

The overall results of the program were checked against the results of Smith (13) for the case of semi-circular crack, and against Alavi's results (14) for the cases $D=.3$ and $D=.4$. The comparison with Smith is shown in Figure 6. The difference in results for θ/θ_{max} near unity is about 5%. Most of this difference can be attributed to the fact that the front surface grids were not the same. Smith used over 500 rectangles on the front surface while this study used 184 rectangles for the first iteration and 62 rectangles for subsequent iterations. The close agreement between these two studies tends to indicate that the iteration procedure is not very sensitive to the surface grid used. The comparison with Alavi's results was not plotted in Figure 6 because of the close agreement. For the case $D=.3$ the results were almost identical, and for $D=.4$, Alavi's results were about 2% higher than the results of this study.

4.3 Surface Grids

As mentioned above, two different front surface grids were used. In all cases the 184 rectangle grid was used for the first iteration, and the 62 rectangle grid was used for the following iterations. It was possible to use Sneddon's closed form solution to calculate the front surface stresses on the first iteration because the crack pressure is constant. Sneddon's closed form solution computes stresses at a much faster rate than the numerical method of Chapter II. For this reason, a finer grid could be used without excessive computer time. When Sneddon's closed form solution was used, the run time was about 200 seconds for this iteration. In addition, it is highly desirable to perform the first iteration as accurately as possible

since the stress intensity factor changes by the largest amount on the first iteration. For example, Smith found that for the semi-circular crack the stress intensity factor changed by 14% as a result of the first iteration and by less than 3% on the second iteration. The 184 rectangle grid is shown in Figure 7, and the 62 rectangle grid is shown in Figure 8 and Figure 9.

The back surface which has 32 rectangles is shown in Figure 10. The back surface is always located outside of the crack and never intersects the crack surface. For this reason the back surface is in a region of low stress gardients, and a fine mesh is not required. Smith and Alavi (15) calculated the stress intensity factor due to a free surface located outside of the crack surface using 64 rectangles on the free surface. To check the 32 rectangle grid some of the cases presented by Smith and Alavi were rerun. The difference between the results was virtually zero.

4.4 The Fourier Series for Crack Pressure

The crack pressure is approximated by a Fourier series in the θ direction and a power series in the r direction. See equations (2.3.3) and (2.4.1). As previously mentioned, the crack surface is represented as an array of points where the crack residual stress has been calculated at each of these points. The Fourier coefficients are determined by numerically integrating over the array's 19 anular divisions for each of the 7 radial divisions, then a least-square curve fit is performed to obtain the power series coefficients of equation (2.4.1). Terms of up to $\cos(5\theta)$ were included in the Fourier series and terms up to r^4 were used in the power series.

In order to realize the benefit of the 184 rectangle grid, and the closed form solution for the first iteration, the stress intensity factor must be calculated with maximum accuracy. The equation for stress intensity factor (2.7.2) shows that this can be accomplished by increasing the number of terms in the crack pressure series. For this reason the Fourier series used terms up to $\cos(10\theta)$ and the power series included terms up to r^5 for calculating the stress intensity factor due to the first iteration. This improved approximation of the crack pressure was not used to compute the stresses for the next iteration, because the circular crack solution can only handle terms up to $\cos(5\theta)$. This means that after the first iteration the crack pressure was approximated with a Fourier-power series containing terms up to $\cos(5\theta)$ and r^4. This less accurate approximation for the crack pressure is considered adequate because the second iteration changes the results by less than 3%.

CHAPTER V

RESULTS

PART I

5.1 General Remarks

For all of the results contained herein the iteration cycle was as follows:

1. One iteration was performed on the front surface using the 184 rectangle grid of Figure 7. The stress intensity factor was calculated using 11 terms in the Fourier series and 6 terms in the power series.
2. A second iteration was performed on the front surface using the 62 rectangle grid of Figure 8 and Figure 9. The pressure distribution was approximated with 6 terms in the Fourier series and 5 terms in the power series. The stress intensity factor was calculated using this same series. For the cases $D = 0, .3, .5, .7$ the iteration cycle was stopped at this point to give the solution for the circular crack partially embedded in a half space.
3. For $D = .2, .4, .6$ the iteration cycle continued with two iterations between the back surface and the crack using the grid of Figure 10. The Fourier series contained 6 terms and the power series had 5 terms.

4. The iteration cycle continued with one additional iteration on each surface and then stopped.

It is possible to approximate the semi-elliptical surface flaw with a partially embedded circular crack. This can be accomplished several different ways, but in this work the comparison will be based on matching the curvature of the ellipse to that of the circular flaw for the same crack depth "A". This comparison is shown in Figure 11. This approximation will be used later to compare the results of this study with experimental data.

5.2 The Results

Figure 6 shows the stress intensity factor for the partially embedded circular crack. The calculated points through which the curves are drawn indicate an increasing tendency to wiggle with increasing D. This would be expected since K_I is approximated by a truncated Fourier series and as D increases θ_{max} decreases, and therefore the lower order harmonics have less effect. The curves show the anticipated trend of decreasing stress intensity factor with decreasing crack depth. The trend of decreasing stress intensity factor with increasing θ/θ_{max} for higher D values is not unexpected. Smith (24) noted the same trend for the semi-elliptical surface flaw. It would be dangerous to put too much faith in the results for θ/θ_{max} near unity because this region is one of high stress gradients due to the singularity at the crack tip. In addition, the surface grid in this region is relatively coarse. The comparison of the D=0 case for this study with the results of Smith (13) also tends to indicate an increased error in this region. However, the area of greatest

interest is near $\theta=0$, because this is the point at which the maximum stress intensity occurs for most crack geometries.

Figure 12 through Figure 14 shows the effect of the back surface for D values of .2, .4, and .6 respectively. The results show the expected trend of increasing stress intensity factor as the back surface moves closer to the crack tip.

Figure 15 is a plot of the back surface intensification factor plotted as a function of D and A/T . This factor is defined as

$$M_t = \frac{K_I}{(K_I \text{ at } A/T = 0)} \qquad \text{for } \theta = 0 \qquad (5.2.1)$$

The real test of an analytical study is a comparison with experimental data. This comparison is presented in Figure 16 and Figure 17. The data was taken from the work of Larson (25). The material used in Larson's work was a brittle epoxy into which semi-elliptical surface flaws were placed. The comparison between the experimental data and the theory is excellent.

CONCLUSION TO PART I

The problem of the circular crack partially embedded in a solid of finite thickness has been solved. The stress intensity factor has been determined for a variety of depths, D, and A/T ratios under uniform tension loading. During the course of the solution a numerical integration technique was devised to calculate the stress in the neighborhood of a circular crack where the crack surface is loaded by a normal pressure $P(r,\theta)$ which can be specified by a Fourier-power series in which terms up to $\cos(5\theta)$ and r^4 are retained. In addition, the stresses on the plane of the crack have been determined in closed form.

The stress intensity factor has been determined as a function of position around the crack front for the crack embedded a depth D, where D varied from 0 to .7 and for A/T ratios from 0 to .85. The results indicate that for deep cracks the back surface can raise the stress intensity factor by as much as 30%. These results are compared with experimental data for semi-elliptical surface flaw cracks. The comparison has been made by matching the curvature of an ellipse to that of the part-circular crack for a given crack depth A. The experimental data scatter about the theoretical results and give a good comparison.

Although all of the results presented here have been for the special case of Poisson's ratio equal to .25 the program is set up in

such a manner that other values of Poisson's ratio can be used. In addition, the program is not restricted to the special case of uniform tension. Any loading which can be approximated with the truncated Fourier-power series can be run with the program.

PART II

INTRODUCTION

There are solutions to many two dimensional crack problems in linear elastic fracture mechanics (5). These solutions generally involve the requirement that the loading causes the crack surfaces to move apart. In this portion of the thesis a solution for a two dimensional through crack is presented in which the requirement of crack surface separation has been relaxed. This type of fracture problem does not appear to have been discussed to any great extent in the literature. Burniston (26) has solved the partially closed Griffith crack for the case where the crack is closed at its center. However, a crack which is closed at one end is of more practical importance, since this could occur with a crack located in a bending field. A typical example of this situation is shown in Figure 18.

Consider the specific problem of a crack located at the center of a pure bending stress field. For this case the existing theory can be used to obtain an upper and lower bound for the stress intensity factor. The upper bound is found by loading the crack shown in Figure 18 with the linear load $P'(y) = \alpha_1 a_o - \alpha_1 y$, where α_1 is the bending load intensity in psi/in. For this loading the stress intensity factor can be calculated using equation 33 on page 37 of reference (5). This computation gives

$$K_I = \frac{3}{2} \alpha_1 a_o \sqrt{\pi a_o}$$

A lower bound for the stress intensity factor can be found by assuming that the crack of Figure 18 is open over one half of its length. The lower bound for the stress intensity factor is given by

$$K_I = \frac{1}{2\sqrt{2}} \cdot \frac{3}{2} \alpha_1 a_o \sqrt{\pi a_o}$$

The upper and lower bounds differ by a factor of $2\sqrt{2}$. In Chapter 9 this problem will be solved using the theory presented here and it will be determined that the actual stress intensity factor is about 80% of the upper bound.

It is the objective of this portion of the thesis to determine the stress intensity factor for a partially closed Griffith crack subjected to a general load specified by a polynomial. This solution will be restricted to the case where the crack has only one open region.

CHAPTER VI

THE PROBLEM

Consider an infinite two-dimensional, linear elastic, homogeneous, isotropic material which has a through Griffith crack. The loading on the material is specified in the form of a polynomial such that the crack opens only once. The problem geometry is shown in Figure 18.

The boundary conditions for this problem may be written as follows:

1. $\sigma_{xx}\Big|_{x=0} = 0$ inside the open portion of the crack;

   $U\Big|_{x=0} = 0$ outside the open portion of the crack;

   $\tau_{xy}\Big|_{x=0} = 0$ all along $x=0$ since only symmetric loads will be considered.

2. For large x and y all stresses must approach the loading stress $P'(y)$.

3. The stress at the closed end of the crack is finite.

A classical approach to this type of problem is to remove the crack and solve the resulting elasticity problem. Then a second problem is formulated such that when these two problems are superimposed the solution to the original problem is obtained.

Figure 19 illustrates how this technique is used to solve the problem of the partially closed crack. Problem A is the problem which results from removing the crack from the original problem. In the sketch of problem B it can be seen that the loading $-P(y)$ is applied to the area where the crack is to be located. In problem A, $+P(y)$ is the stress at this same location so that superposition then gives the boundary conditions of the original problem.

Problem A is a typical elasticity problem and can be solved by many different methods. Problem B is a mixed boundary value problem and its solution will be developed in the next chapter.

CHAPTER VII

THE MIXED BOUNDARY VALUE PROBLEM

7.1 Boundary Conditions

The boundary conditions for the mixed boundary value problem can be stated as follows:

$$\text{a.} \quad \sigma_{xx}\Big|_{x=0} = -P(y) \qquad \text{for} \quad |y| \leq a \qquad (7.1.1a)$$

$$\text{b.} \quad \dot{U}\Big|_{x=0} = 0 \qquad \text{for} \quad |y| > a \qquad (7.1.1b)$$

$$\text{c.} \quad \tau_{xy}\Big|_{x=0} = 0 \qquad \text{for all} \quad x=0 \qquad (7.1.1c)$$

$$\text{d.} \quad \sigma_{ij} \to 0 \quad \text{as} \quad x \to \infty \qquad (7.1.1d)$$

e. On an intuitive basis, the boundary condition at the closed end of the crack is

$$K_I = \lim_{y \to a} \sqrt{2\pi(y-a)} \; \sigma_{xx}\Big|_{x=0} = 0 \qquad (7.1.1e)$$

This supposition is easily verified by considering the alternate possibilities: Suppose that $K_I < 0$, then calculation of the crack opening displacement shows that the crack surface has deflected through itself, which is impossible. Suppose that $K_I > 0$, then from the definition of stress intensity factor the stress $\sigma_{xx} > 0$ at $x=0$ and

y=a, which is also impossible because the physical crack extends past y=a and cannot support a tension stress. The only remaining alternative is that $K_I = 0$. The problem geometry is illustrated in Figure 20.

7.2 The Potential Formulation

For the case of plain strain the Navier equations take the form

$$\nabla^2 U + \frac{1}{(1-2\nu)} \frac{\partial}{\partial x} \left\{ \frac{\partial U}{\partial x} + \frac{\partial V}{\partial y} \right\} = 0$$

$$\nabla^2 V + \frac{1}{(1-2\nu)} \frac{\partial}{\partial y} \left\{ \frac{\partial U}{\partial x} + \frac{\partial V}{\partial y} \right\} = 0 \qquad (7.2.1)$$

where U = displacement in the x direction

V = displacement in the y direction

ν = Poisson's ratio.

For the class of problems in which the shearing stresses vanish at all points on the plane $x=0$ the following potential formulation satisfies Navier's equations (7.2.1).

$$U = -\beta^2 \frac{\partial \phi}{\partial x} + (\beta^2-1)\, x \frac{\partial^2 \phi}{\partial x^2}$$

$$V = \frac{\partial \phi}{\partial y} + (\beta^2-1)\, x \frac{\partial^2 \phi}{\partial x^2} \qquad (7.2.2)$$

$$\beta^2 = \frac{2(1-\nu)}{(1-2\nu)}$$

Provided that ϕ satisfies $\nabla^2 \phi = 0$

The above displacements U and V have been nondimensionalized with respect to the crack radius "a".

Using Hooke's law the stress components in terms of the potential function ϕ are found to be:

$$\sigma_{xx} = -2(\beta^2-1)\frac{\partial^2\phi}{\partial x^2} + 2(\beta^2-1)\,x\,\frac{\partial^3\phi}{\partial x^3}$$

$$\sigma_{yy} = -2(\beta^2-1)\frac{\partial^2\phi}{\partial x^2} - 2(\beta^2-1)\,x\,\frac{\partial^3\phi}{\partial x^3} \qquad (7.2.3)$$

$$\tau_{xy} = 2(\beta^2-1)\,x\,\frac{\partial^3\phi}{\partial x^2\partial y}$$

These stresses have been nondimensionalized through division by G, the shear modulus.

The boundary conditions (7.1.1a&b) now take the form

$$\frac{\partial^2\phi}{\partial x^2} = \frac{P(y)}{2(\beta^2-1)} \qquad |y| \le a \qquad (7.2.4a)$$

$$\frac{\partial\phi}{\partial x} = 0 \qquad |y| > a \qquad (7.2.4b)$$

The boundary condition (7.1.1c) is automatically satisfied by the potential formulation.

7.3 The Potential Function

To satisfy the mixed boundary conditions of equations (2.2.4a and b) a potential function will be assumed in the form

$$\phi = \frac{1}{2(\beta^2-1)} \int_0^\infty \frac{f(\xi)}{\xi} \cos(\xi y)\, e^{-\xi x}\, d\xi + \frac{1}{2(\beta^2-1)} \times$$

$$\int_0^\infty \frac{g(\xi)}{\xi} \sin(\xi y)\, e^{-\xi x}\, d\xi \qquad (7.3.1)$$

Potential functions in this form have been used by Sneddon (27) to solve related problems in fracture mechanics. From the form of ϕ it is clear that Laplace's equation is satisfied, and that for large x values σ_{ij} tends toward zero.

Substitution of the above ϕ function into the boundary conditions (2.2.4a and b) gives the following set of integral equations:

$$P(y) = \int_0^\infty \xi\, f(\xi) \cos(\xi y)\, d\xi$$

$$+ \int_0^\infty \xi\, g(\xi) \sin(\xi y)\, d\xi \quad , \quad |y| \le a \qquad (7.3.2)$$

$$0 = \int_0^\infty f(\xi) \cos(\xi y)\, d\xi$$

$$+ \int_0^\infty g(\xi) \sin(\xi y)\, d\xi \quad , \quad |y| > a \quad . \qquad (7.3.3)$$

Now if $P(y)$ is divided into a symmetric and an anti-symmetric function, the above integral equations may be rewritten as a pair of dual integral equations.

The symmetric portion gives the following set of dual integral equations:

$$P_s(y) = \int_0^\infty \xi\, f(\xi) \cos(\xi y)\, d\xi \quad , \quad |y| \le a \qquad (7.3.4)$$

$$0 = \int_0^\infty f(\xi) \cos(\xi y)\, d\xi \quad , \quad |y| > a \qquad (7.3.5)$$

where $P_s(y)$ is the symmetric portion of $P(y)$.

The anti-symmetric portion gives the pair of dual integral equations:

$$P_a(y) = \int_0^\infty \xi\, g(\xi) \sin(\xi y)\, d\xi \quad , \quad |y| \le a \qquad (7.3.6)$$

$$0 = \int_0^\infty g(\xi) \sin(\xi y)\, d\xi \quad , \quad |y| > a \qquad (7.3.7)$$

where $P_a(y)$ is the anti-symmetric portion of $P(y)$.

The solution to the above dual integral equations, due to Busbridge, is given by Sneddon in (18).

The relationships which give $f(\xi)$ and $g(\xi)$ are

$$f(\xi) = \frac{2}{\pi} \int_0^a \eta J_0(\xi\eta) d\eta \int_0^\eta \frac{P_s(\rho)}{\sqrt{\eta^2 - \rho^2}}\, d\rho \qquad (7.3.8)$$

$$g(\xi) = \frac{2}{\pi} \int_0^a J_1(\xi\lambda) d\lambda \int_0^\lambda \frac{\rho\, P_a(\rho)}{\sqrt{\lambda^2 - \rho^2}}\, d\rho \qquad (7.3.9)$$

With the functions $f(\xi)$ and $g(\xi)$ known, the potential function ϕ is completely determined except that "a", the open-portion crack length is still unknown. To determine "a", the boundary condition $K_I = 0$ at the closed end of the crack (2.1.1e) will be used. However, this will not be done until after the σ_{xx} stress component has been computed.

CHAPTER VIII

THE STRESS AND DISPLACEMENT

8.1 The Stress and Displacement Functions

To determine the stress and displacement on the plane $x=0$ the functions $f(\xi)$ and $g(\xi)$, (7.3.8) and (7.3.9), are substituted into the potential function ϕ and then the formulas (7.2.2) and (7.2.3) are used to calculate the stress and displacement. This computation gives

$$\sigma_{xx}\Big|_{x=0} = -\int_0^\infty \left\{\frac{2}{\pi}\int_0^a \eta\, J_o(\xi\eta)\, d\eta \times \int_0^\eta \frac{P_s(\rho)}{\sqrt{\eta^2-\rho^2}}\, d\rho\right\} \xi \cos(\xi y)\, d\xi$$

$$\int_0^\infty \left\{\frac{2}{\pi}\int_0^a J_1(\xi\lambda)\, d\lambda \int_0^\lambda \frac{\rho\, P_a(\rho)}{\sqrt{\lambda^2-\rho^2}}\, d\rho\right\} \times \xi \sin(\xi y)\, d\xi \qquad \text{for } |y| > a \quad (8.1.1)$$

and

$$U\Big|_{x=0} = -\frac{\beta^2}{2(\beta^2-1)}\int_0^\infty \left\{\frac{2}{\pi}\int_0^a \eta\, J_o(\xi\eta)\, d\eta \times \int_0^\eta \frac{P_s(\rho)}{\sqrt{\eta^2-\rho^2}}\, d\rho\right\} \cos(\xi y)\, d\xi$$

$$- \frac{\beta^2}{2(\beta^2-1)} \int_0^{\infty} \left\{ \frac{2}{\pi} \int_0^{a} J_1(\xi\lambda)\, d\lambda \times \right.$$

$$\left. \int_0^{\lambda} \frac{\rho\, P_a(\rho)}{\sqrt{\lambda^2 - \rho^2}}\, d\rho \right\} \sin(\xi y)\, d\xi \qquad (8.1.2)$$

$$\text{for } |y| \leq a$$

Before the above integrations can be completed the form of the loading function $P(y)$ must be known. To make the integrations as simple as possible the loading function will be assumed in the form of a polynomial.

8.2 The Loading Function P(y)

The loading must be specified as some function in the x,y coordinate system of Figure 18. However, the loading is known only in terms of some material reference frame. For this problem the material reference frame is located at the center fo the physical crack and is designated x', y' in Figure 18. In terms of the x', y' coordinate system the loading function may be written as

$$P(y') = \alpha_o + \alpha_1 y' + \alpha_2 y' + \ldots + \alpha_K y'^K$$

$$P(y') = \sum_{n=0}^{K} \alpha_n y'^n \qquad (8.2.1)$$

From Figure 18 it is clear that

$$y' = y - (a_o - a)$$

With this relationship the loading function may be written in the form

$$P(y) = \sum_{m=0}^{K} \beta_m y^m \tag{8.2.2}$$

where $$\beta_m = \sum_{n=m}^{K} \alpha_n \binom{n}{m} (a - a_o)^{n-m} \tag{8.2.3}$$

and $\binom{n}{m}$ are the binomial coefficients.

Now the loading function may be broken into an even and an odd function to give

$$P_s(y) + P_a(y) = \sum_{m=0}^{H} \beta_{2m} y^{2m} + \sum_{m=1}^{J} \beta_{2m-1} y^{2m-1} \tag{8.2.3}$$

where H+1 is the number of even terms in the loading function and J is the number of odd terms.

8.3 Integrated Form of the Stress and Displacements

Now that the polynomial form of P(y) has been established the expression for stress and displacement can be determined. Denoting the second term of equation (8.1.1) by "I" and then rewriting it gives

$$I = -\frac{2}{\pi} \int_0^a d\lambda \int_0^\lambda \frac{\rho\, P_a(\rho)\, d\rho}{\sqrt{\lambda^2 - \rho^2}} \int_0^\infty \xi \sin(\xi y)\, J_1(\xi\lambda)\, d\xi \tag{8.3.1}$$

Making use of the relationship

$$\frac{d}{d\lambda} [J_o(\xi\lambda)] = - J_1(\xi\lambda)\, \xi \tag{8.3.2}$$

The infinite integral may be rewritten as

$$I = -\frac{2}{\pi} \int_0^a d\lambda \int_o^\lambda \frac{\rho\, P_a(\rho)\, d\rho}{\sqrt{\lambda^2 - \rho^2}} \left\{ -\frac{d}{d\lambda} \int_0^\infty J_o(\xi\lambda) \sin(\xi y)\, d\xi \right\} \tag{8.3.3}$$

Watson (20) gives the value for this infinite integral, which is a special case of the Weber-Schafheitlin integral, as

$$\int_0^\infty J_o(\xi\lambda) \sin(\xi y)\, d\xi = \frac{1}{\sqrt{y^2 - \lambda^2}} \quad \text{for} \quad \lambda < y \tag{8.3.4}$$

Substitution of this result into equation (8.3.3) gives

$$I = \frac{2}{\pi} \int_0^a \frac{\lambda\, d\lambda}{(y^2 - \lambda^2)^{3/2}} \int_0^\lambda \frac{\rho\, P_a(\rho)\, d\rho}{\sqrt{\lambda^2 - \rho^2}} \tag{8.3.5}$$

From equation (8.2.4) $P_a(\rho)$ can be written

$$P_a(\rho) = \sum_{m=1}^{J} \beta_{2m-1}\, \rho^{2m-1} \tag{8.3.6}$$

Substitution of $P_a(\rho)$ into (8.3.5) gives

$$I = \frac{2}{\pi} \int_0^a \frac{\lambda\, d\lambda}{(\lambda^2 - \rho^2)^{3/2}} \sum_{m=1}^{J} \beta_{2m-1} \int_0^\lambda \frac{\rho^{2m}}{\sqrt{\lambda^2 - \rho^2}}\, d\rho \tag{8.3.7}$$

The last integral in (8.3.7) has the value

$$\int_0^\lambda \frac{\rho^{2m}}{\sqrt{\lambda^2 - \rho^2}}\, d\rho = \frac{\sqrt{\pi}}{2} \frac{\Gamma(m+\frac{1}{2})}{\Gamma(m+1)} \lambda^{2m}, \quad 2m \geq 1 \tag{8.3.8}$$

Substitution of this result into the expression (8.3.7) results in the term

$$I = \frac{1}{\sqrt{\pi}} \sum_{m=1}^{J} \beta_{2m-1} \frac{\Gamma(m+\frac{1}{2})}{\Gamma(m+1)} \int_0^a \frac{\lambda^{2m+1}}{(y^2-\lambda^2)^{3/2}} d\lambda \qquad (8.3.9)$$

Using a similar procedure on the remaining terms in equations (8.1.1) and (8.1.2), it follows that the stress on the plane $x=0$ is given by

$$\sigma_{xx}\Big|_{x=0} = \beta_o \left\{ \frac{y - \sqrt{y^2-a^2}}{\sqrt{y^2-a^2}} \right\}$$

$$+ \frac{y}{\sqrt{\pi}} \sum_{m=1}^{H} \beta_{2m} \frac{\Gamma(m+\frac{1}{2})}{\Gamma(m+1)} \int_0^a \frac{\eta^{2m+1}\, d\eta}{(y^2-a^2)^{3/2}}$$

$$+ \frac{1}{\sqrt{\pi}} \sum_{m=1}^{J} \beta_{2m-1} \frac{\Gamma(m+\frac{1}{2})}{\Gamma(m+1)} \int_0^a \frac{\lambda^{2m+1}\, d\lambda}{(y^2-\lambda^2)^{3/2}}$$

$$\text{for} \quad |y| > a$$

$$\sigma_{xx}\Big|_{x=0} = P(y) \qquad \text{for} \quad |y| < a \qquad (8.3.10)$$

and the displacement on the plane $x=0$ is given by the expression

$$U\Big|_{x=0} = \frac{(1-\nu)}{\sqrt{\pi}} \left\{ \sum_{m=0}^{H} \beta_{2m} \frac{\Gamma(m+\frac{1}{2})}{\Gamma(m+1)} \int_y^a \frac{x^{2m+1}}{\sqrt{x^2-y^2}} dx \right.$$

$$\left. + \sum_{m=1}^{J} \beta_{2m-1} \frac{\Gamma(m+\frac{1}{2})}{\Gamma(m+1)} y \int_y^a \frac{x^{2m-1}}{\sqrt{x^2-y^2}} dx \right\} \quad \text{for } |y| \le a$$

$$U\Big|_{x=0} = 0 \quad \text{for} \quad |y| \ge a \qquad (8.3.10)$$

The following three integration formulas will be used to obtain the final expression for stress and displacement:

$$\int_y^a \frac{x^{2m+1}}{\sqrt{x^2-y^2}}\,dx = \sqrt{a^2-y^2} \sum_{k=0}^{m} \binom{m}{k} \frac{(a^2-y^2)^{m-k}}{[2(m-k)+1]}\, y^{2k} \qquad (8.3.12)$$

for $m \geq 0$

$$y \int_y^a \frac{x^{2m-1}}{\sqrt{x^2-y^2}}\,dx = \sqrt{a^2-y^2} \sum_{k=0}^{m-1} \binom{m-1}{k} \frac{(a^2-y^2)^{m-k-1}}{[2(m-k)-1]}\, y^{2k+1} \qquad (8.8.13)$$

for $m \geq 1$

$$\int_o^a \frac{x^{2m+1}}{(y^2-x^2)^{3/2}}\,dx = \frac{a^{2(m+1)}}{y^2\sqrt{y^2-a^2}} + \frac{(2m+1)}{y} \sum_{k=0}^{m} \frac{\binom{m}{k}(-1)^k}{[2(m+k)+1]} \times \left[(y^2-a^2)^{m-k+\frac{1}{2}}\, y^{2k-1} - y^{2m}\right] \qquad (8.3.14)$$

for $m \geq 0$

Now the stress on the plane $x=0$ can be written as

$$\sigma_{xx}\Big|_{x=0} = \frac{a^3}{y^2\sqrt{\pi}\sqrt{y^2-a^2}} \left\{ \beta_o\, y^3 \frac{\sqrt{\pi}}{a^3} + y \sum_{m=1}^{H} \beta_{2m} \frac{\Gamma(m+\frac{1}{2})}{\Gamma(m+1)}\, a^{2m-1} + \sum_{m=1}^{J} \beta_{2m-1} \frac{\Gamma(m+\frac{1}{2})}{\Gamma(m+1)}\, a^{2m-1} \right\} - \beta_o + \frac{1}{\sqrt{\pi}} \sum_{m=1}^{H} \beta_{2m} \times \frac{\Gamma(m+\frac{1}{2})}{\Gamma(m+1)} (2m+1) \sum_{k=0}^{m} \frac{\binom{m}{k}(-1)^k}{[2(m-k)+1]} \left[(y^2-a^2)^{m-k+\frac{1}{2}} y^{2k} - y^{2m}\right] + \frac{1}{\sqrt{\pi}} \sum_{m=1}^{J} \beta_{2m-1} \frac{\Gamma(m+\frac{1}{2})}{\Gamma(m+1)} \frac{(2m+1)}{y} \sum_{k=0}^{m} \frac{\binom{m}{k}(-1)^k}{[2(m-k)+1]} \times$$

$$\left[(y^2-a^2)^{m-k+\frac{1}{2}}\, y^{2k} - y^{2m}\right] \qquad \text{for} \quad |y| \geq a$$

and $$\sigma_{xx}\Big|_{x=0} = P(y) \qquad \text{for} \quad |y| < a .$$

The displacements take the form

$$U\Big|_{x=0} = \frac{(1-\nu)}{\sqrt{\pi}} \sqrt{a^2-y^2} \left\{ \sum_{m=0}^{H} \beta_{2m} \frac{\Gamma(m+\frac{1}{2})}{\Gamma(m+1)} \sum_{k=0}^{m} \frac{\binom{m}{k} (a^2-y^2)^{m-k} y^{2k}}{[2(m-k)+1]} \right.$$

$$\left. + \sum_{m=1}^{J} \beta_{2m-1} \frac{\Gamma(m+\frac{1}{2})}{\Gamma(m+1)} \sum_{k=0}^{m-1} \frac{\binom{m-1}{k} (a^2-y^2)^{m-k-1} y^{2k+1}}{[2(m-k)-1]} \right\}$$

$$\text{for} \quad |y| \leq a$$

and $$U\Big|_{x=0} = 0 \qquad \text{for} \quad |y| > a$$

8.4 The Open Crack Length "a"

The only remaining unknown is the open crack length "a". To determine "a" the last boundary condition, $K_I = 0$ at the closed end of the crack (7.1.1e) will be used. This condition may be written as

$$\lim_{y \to a} \sqrt{2\pi(y-a)} \quad \sigma_{xx}\Big|_{x=0} = 0 \qquad (8.4.1)$$

To simplify the equations the stress will be written in the following symbolic form:

$$\sigma_{xx}\Big|_{x=0} = \frac{\left[\dfrac{a}{\sqrt{\pi}\, y^2 \sqrt{y+a}}\right]}{\sqrt{y-a}} H(y) + G(y) \qquad (8.4.2)$$

where

$$H(y) = \beta_o y^3 \frac{\sqrt{\pi}}{a^3} + y \sum_{m=1}^{H} \beta_{2m} \frac{\Gamma(m+\frac{1}{2})}{\Gamma(m+1)} a^{2m-1}$$

$$+ \sum_{m=1}^{J} \beta_{2m-1} \frac{\Gamma(m+\frac{1}{2})}{\Gamma(m+1)} a^{2m-1} \qquad (8.4.3)$$

and

$$G(y) = -\beta_o + \frac{1}{\sqrt{\pi}} \sum_{m=1}^{H} \beta_{2m} \frac{\Gamma(m+\frac{1}{2})}{\Gamma(m+1)} (2m+1) \sum_{k=0}^{m} \frac{\binom{m}{k} (-1)^k}{[2(m-k)+1]} \times$$

$$\left[(y^2-a^2)^{m-k+\frac{1}{2}} y^{2k-1} - y^{2m}\right] + \frac{1}{\sqrt{\pi}} \sum_{m=1}^{J} \beta_{2m-1} \times$$

$$\frac{\Gamma(m+\frac{1}{2})}{\Gamma(m+1)} \frac{(2m+1)}{y} \sum_{k=0}^{m} \frac{\binom{m}{k} (-1)^k}{[2(m-k)+1]} \times$$

$$\left[(y^2-a^2)^{m-k+\frac{1}{2}} y^{2k-1} - y^{2m}\right] \qquad (8.4.4)$$

With the substitution of the symbolic form for σ_{xx} into the boundary condition (8.4.1) the following requirement results

$$\lim_{y \to a} \sqrt{2\pi(y-a)} \left\{ \left[\frac{\frac{a^3}{\sqrt{\pi}\, y^2 \sqrt{y+a}}}{y-a} \right] H(y) + G(y) \right\} = 0 \qquad (8.4.5)$$

Careful examination of equations (8.4.3) and (8.4.4) shows that both $H(y)$ and $G(y)$ are finite at $y=a$. Therefore, to satisfy equation (8.4.5) $H(y)$ must be factorable into the form

$$H(y) = (y-a)\, Q(y) \qquad (8.4.6)$$

If $H(y)$ is factorable into the form shown in equation (8.4.6) then

$$H(a) = \sum_{m=0}^{H} \beta_{2m} \frac{\Gamma(m+\frac{1}{2})}{\Gamma(m+1)} a^{2m} + \sum_{m=1}^{J} \beta_{2m-1} \frac{\Gamma(m+\frac{1}{2})}{\Gamma(m+1)} a^{2m-1} = 0 \qquad (8.4.7)$$

and the open crack length "a" is found to be one of the roots of the equation $H(a) = 0$.

8.5 Admissible Roots

Some of the roots of $H(a) = 0$ are not admissible as values for "a". For example, complex roots have no physical meaning. Referring to Figure 18, the following statements can be made:

1. One real root on $[0 , a_o]$ and, or one real root on $[0 , -a_o]$ is allowable. This restriction must be imposed because the initial formulation was made assuming that the crack opened only once.
2. Roots where $|a| > |a_o|$ have no physical interpretation.
3. Complex roots have no physical interpretation.

The solution to the partially closed crack is now complete, however, one additional point will be investigated before proceeding to an example.

8.6 Slope at the Closed End of the Crack

For the Penny shaped crack, Emery and Smith (27) found that when $K_I = 0$ the slope of the crack opening shape was zero at the crack tip. Similar results can be expected here. This can be written in equation form as

$$\left.\frac{\partial U}{\partial y}\right|_{\substack{x=0\\y=a}} = 0 \qquad (8.6.1)$$

In this section it will be shown that this conjecture is true.

The first step is to take the derivative of U with respect to y. This computation gives

$$\left.\frac{\partial U}{\partial y}\right|_{x=0} = \frac{y}{\sqrt{a^2-y^2}} R(y) + \sqrt{a^2-y^2}\ \frac{dR(y)}{dy} \qquad (8.6.2)$$

where

$$R(y) = \frac{(1-\nu)}{\sqrt{\pi}} \sum_{m=0}^{H} \beta_{2m} \frac{\Gamma(m+\frac{1}{2})}{\Gamma(m+1)} \sum_{k=0}^{m} \frac{\binom{m}{k} (a^2-y^2)^{m-k}\, y^{2k}}{[2(m-k)+1]}$$

$$+ \frac{(1-\nu)}{\sqrt{\pi}} \sum_{m=1}^{J} \beta_{2m-1} \frac{\Gamma(m+\frac{1}{2})}{\Gamma(m+1)} \sum_{k=0}^{m-1} \frac{\binom{m-1}{k} (a^2-y^2)^{m-k-1} y^{2k+1}}{[2(m-k)+1]} \qquad (8.6.3)$$

The next step is to examine the behavior of (8.6.2) as y approaches "a". Since the second term of (8.6.2) goes to zero this leaves

$$\left.\frac{\partial U}{\partial y}\right|_{\substack{x=0\\y=a}} = \lim_{y \to a} \left\{ \frac{y}{\sqrt{a^2-y^2}} \right\} \lim_{y \to a} \left\{ R(y) \right\} \qquad (8.6.4)$$

It can be demonstrated that

$$\lim_{y \to a} R(y) = \frac{(1-\nu)}{\sqrt{\pi}} \left\{ \sum_{m=0}^{H} \beta_{2m} \frac{\Gamma(m+\frac{1}{2})}{\Gamma(m+1)} a^{2m} + \sum_{m=1}^{J} \beta_{2m-1} \frac{\Gamma(m+\frac{1}{2})}{\Gamma(m+1)} a^{2m-1} \right\} \qquad (8.6.5)$$

However, the term in brackets is $H(a)$ which is known to be zero. By summing out $R(y)$ in equation (8.4.3) it can be shown that $R(y)$ is a polynomial in y. Now if the polynomial $R(y)$ is equal to zero at $y = a$, then $R(y)$ is factorable into the form $R(y) = (y-a)B(y)$. Hence, the Limit (8.6.4) can be rewritten and evaluated to give

$$\left.\frac{\partial U}{\partial y}\right|_{\substack{x=0\\y=a}} = \underset{y \to a}{\text{Limit}} \frac{(1-\nu)}{\sqrt{\pi}} \frac{y(y-a)}{\sqrt{a^2-y^2}} B(y) = 0 \qquad (8.6.6)$$

This shows that for a loading function $P(y)$ in the form of a polynomial, if $K_I = 0$ at $y = a$, then $\partial U/\partial y|_{x=0} = 0$ at $y = a$.

CHAPTER IX

AN EXAMPLE PROBLEM

9.1 The Problem of Pure Bending

Consider a bending problem where the applied load, P'(y), of Figure 18, has the form

$$P'(y) = \alpha_o + \alpha_1 y \tag{9.1.1}$$

For this applied load, the loading function P(y) of section 8.2 is given by

$$P(y) = \beta_o + \beta_1 y \tag{9.1.2}$$

where, from (3.2.3)

$$\beta_o = \alpha_o + \alpha_1 (a - a_o) \tag{9.1.3}$$

$$\beta_1 = \alpha_1 \tag{9.1.4}$$

The open crack length "a" is found by substitution into (9.4.7) which gives

$$a = \frac{2}{3} \frac{(\alpha_1 a_o - \alpha_o)}{\alpha_1} \tag{9.1.5}$$

For the special case of pure bending, $\alpha_o = 0$, and then $a = 2/3\ a_o$.

9.2 The Stress and Displacements for Pure Bending

To find the stress and displacements on the plane $x = 0$ requires substitution of β_o and β_1 into equations (8.3.15) and (3.3.16). This substitution gives

$$\sigma_{xx}\Big|_{x=0} = \beta_o\left(\frac{|y|}{\sqrt{y^2-a^2}} - 1\right) \pm \frac{\beta_1}{2}\left(\sqrt{y^2-a^2} + \frac{y^2}{\sqrt{y^2-a^2}} - 2|y|\right) \tag{9.2.1}$$

$$U\Big|_{x=0} = \sqrt{y^2-a^2}\ \left(\beta_o + \beta_1 \frac{y}{2}\right) \tag{9.2.2}$$

Great care must be taken to use the correct sign for the terms which result from the anti-symmetric loading. To calculate the influence of an anti symmetric term for $y < 0$, y is replaced with $|y|$ and then each anti-symmetric term is multiplied by minus one. Equations (9.2.1) and (9.2.2) have been setup in this manner.

Figure 21 is a plot of the stress on the plane $x=0$. This is the stress for the mixed boundary value problem of Chapter VII, which is illustrated in Figure 20.

Figure 23 shows the stress which results from the complete problem as shown in Figure 18. This is the final result for the original problem posed in Chapter VI.

9.3 The Stress Intensity Factor

Substitution of the stress (9.2.1) into equation (2.7.1) for stress intensity factor gives

$$K_I = \underset{y \to a}{\text{Limit}} \left\{ \frac{\sqrt{2\pi}\ \beta_o\ |y|}{\sqrt{y+a}} \pm \beta_1\ \frac{\sqrt{2\pi}\ y^2}{\sqrt{y+a}} \right\} \tag{9.3.1}$$

for $\alpha_o = 0$, then

$$K_I = \alpha_1 \frac{a_o}{3}\sqrt{\frac{2\pi\, a_o}{3}} \pm \alpha_1 \frac{a_o}{3}\sqrt{\frac{2\pi a_o}{3}} \qquad (9.3.2)$$

Then at the closed end of the crack $K_I = 0$ and at the open end of the crack

$$K_I = \frac{2}{3}\alpha_1 a_o \sqrt{\frac{2\pi\, a_o}{3}} \qquad (9.3.3)$$

The stress intensity factor given in equation (9.3.3) is about 80% of the upper bound which was calculated in the introduction to Part II.

CONCLUSION TO PART II

A formulation for the partially closed Griffith crack has been presented. The resulting mixed boundary value problem has been solved. The following results have been obtained:

1. A closed form solution has been obtained for the stress and displacement on the plane $x=0$. In addition, a criterion for determining the open crack length "a" has been presented.
2. These results show that for the closed end of the crack the requirement that the stress intensity factor be zero also requires that the slope of the crack opening shape be zero at that point.
3. To demonstrate the use of these results the problem of pure bending which closed one end of the crack has been solved.

The general form of the results which have been presented here make it possible to solve an entire class of fracture problems where the crack is forced closed at one or both ends.

CONCLUSION TO THE THESIS

The surface crack has often been found to cause the failure of structural components; however, as previously mentioned, only limited analytical work has been done on this problem. This is the first analytical study of a surface crack in a solid of finite thickness. The results of this study can be directly applied to the fracture analysis for brittle materials. This is accomplished by calculating the stress intensity factor from the results presented in Figure 6 and Figure 15.

The design engineer attempting to design against a fracture failure is likely to select a material which is very ductile. In that case plasticity effects would be significant and the results of this study would not be applicable. However, the results of this study together with an experimental program would make it possible to determine the plasticity effects. The results of the experimental program could take the form of a plasticity correction factor which would be applied to the elastic stress intensity factor of this study.

For two dimensional cracks the size of the plastic zone around the crack tip has been estimated using the elastic analysis. This has been accomplished by determining the region in which the elastic analysis indicates that yielding has occurred. In a similar manner, the elastic analysis presented here could be used to approximate the yield zone for a surface crack in a finite solid.

Based on the success of this study it would seem worth while to use this same iteration procedure with the elliptical crack solution (11). In this way, the semi-elliptical crack could be studied directly.

The solution which has been presented for the partially closed Griffith crack extends the theory of linear elastic fracture mechanics to include a new class of problems. The solution here makes it possible to solve the class of problems where the loading closes a portion of the crack. The problem of pure bending which closes one end of the crack is the most common example of this situation. Although the problem of pure bending is the only example which has been worked out here, many different types of problems can be solved with the solution presented. The solution is general because the loading on the crack surface is represented in the form of a polynomial. For example, a thermal stress problem could be solved by approximating the crack surface stresses due to the thermal loading with a polynomial. Then this polynomial would be used as the loading function in the analysis.

The general solutions presented in this thesis represent a significant advance in the theory of fracture mechanics. The results presented here are directly applicable to a wide class of problems, which up to this point have had no analytical solutions.

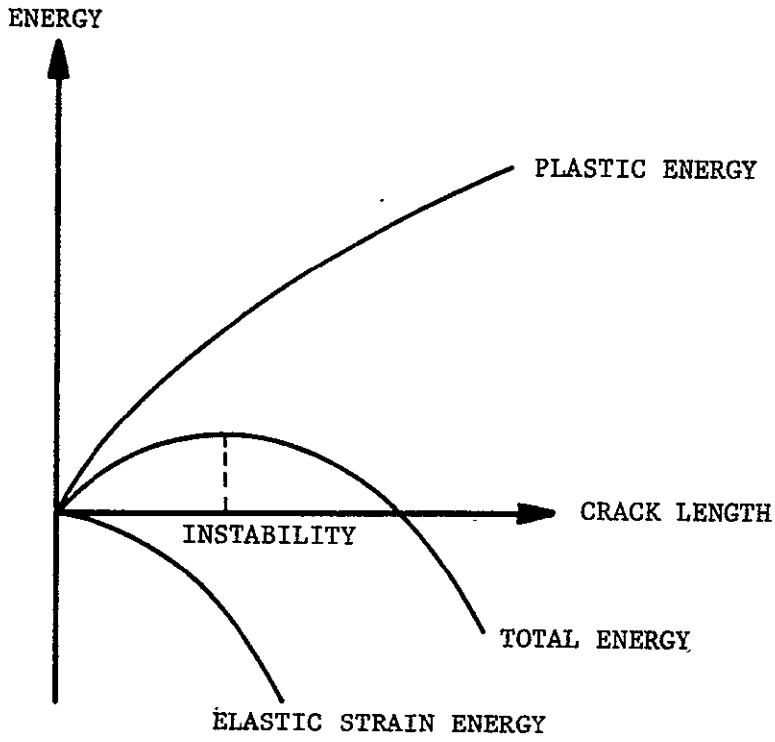

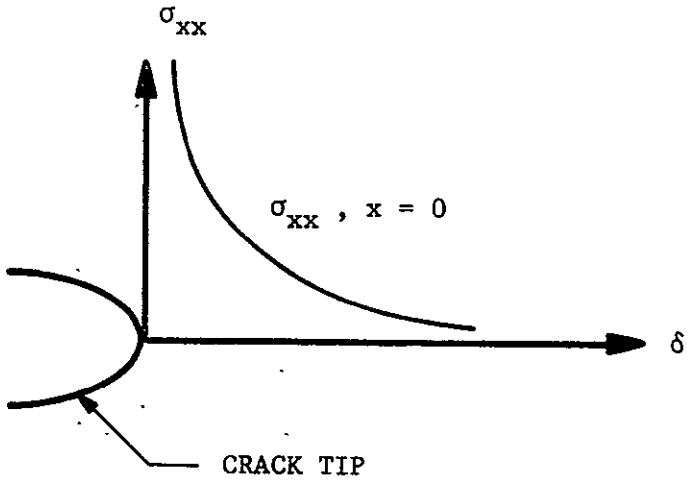

Figure 1.--Irwin-Griffith Energy Balance

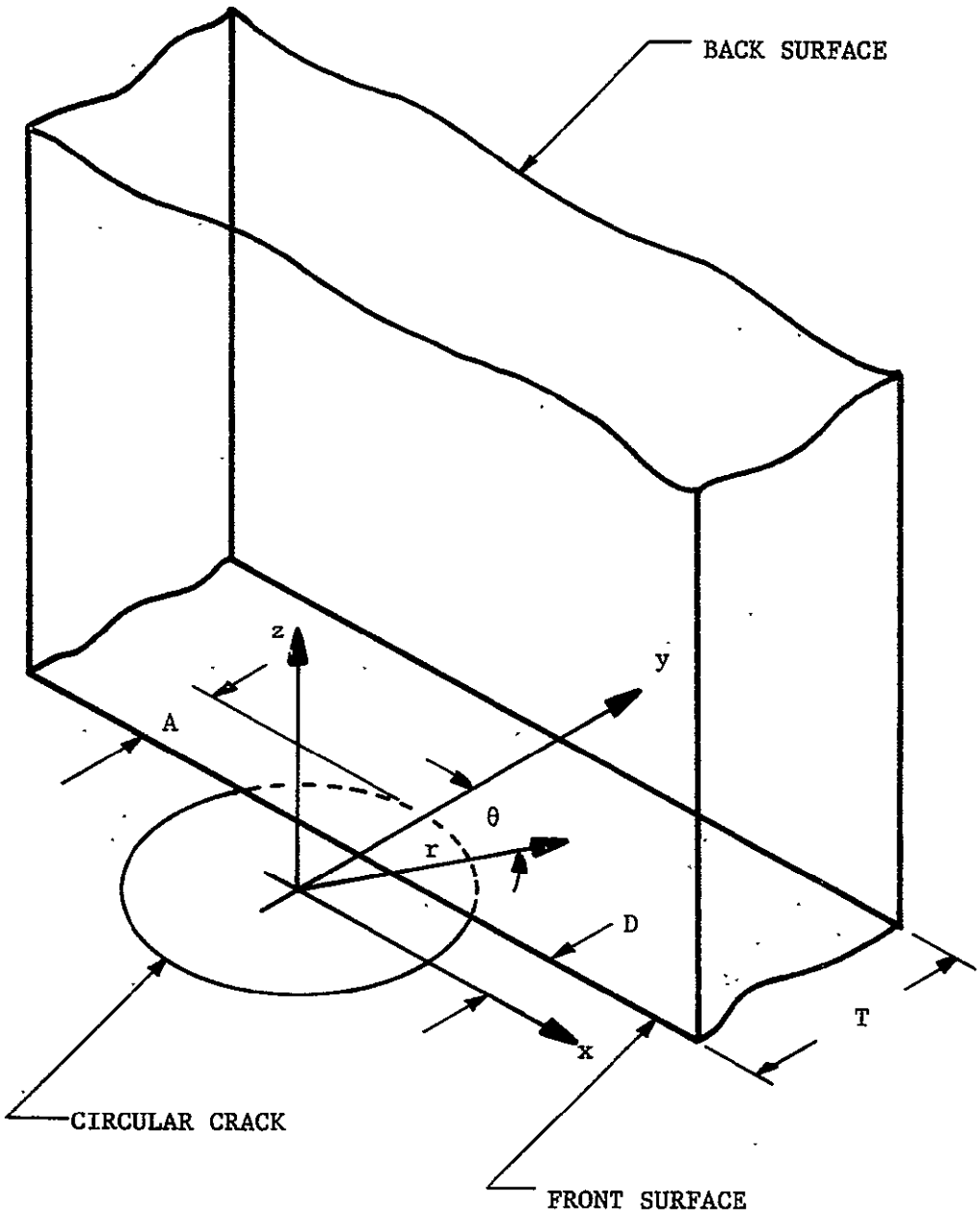

Figure 2.--The Circular Surface Flaw

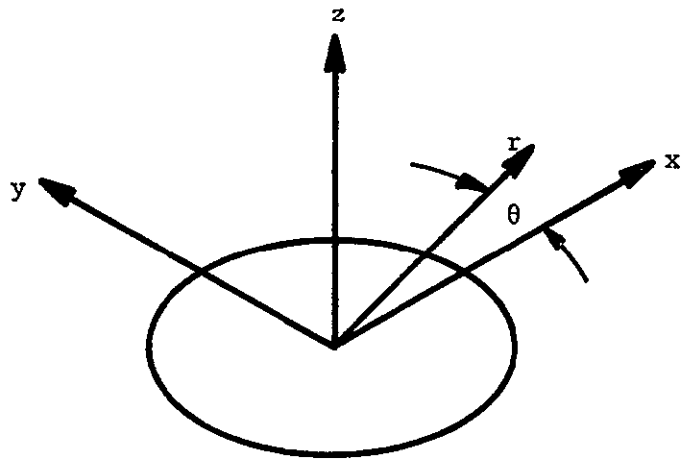

Figure 3.--The Circular Crack in an Infinite Solid

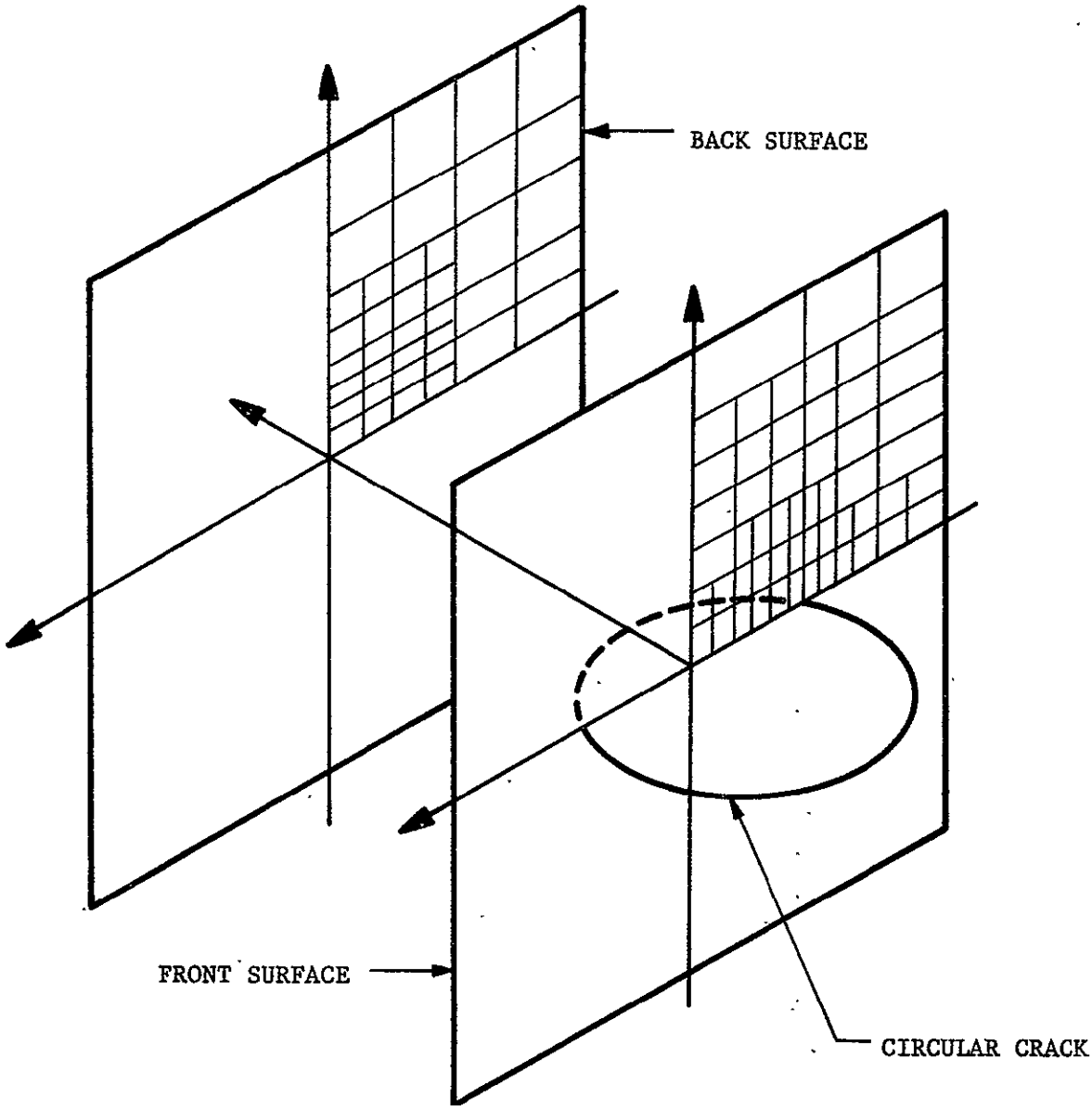

Figure 4.--Setup For the Iteration

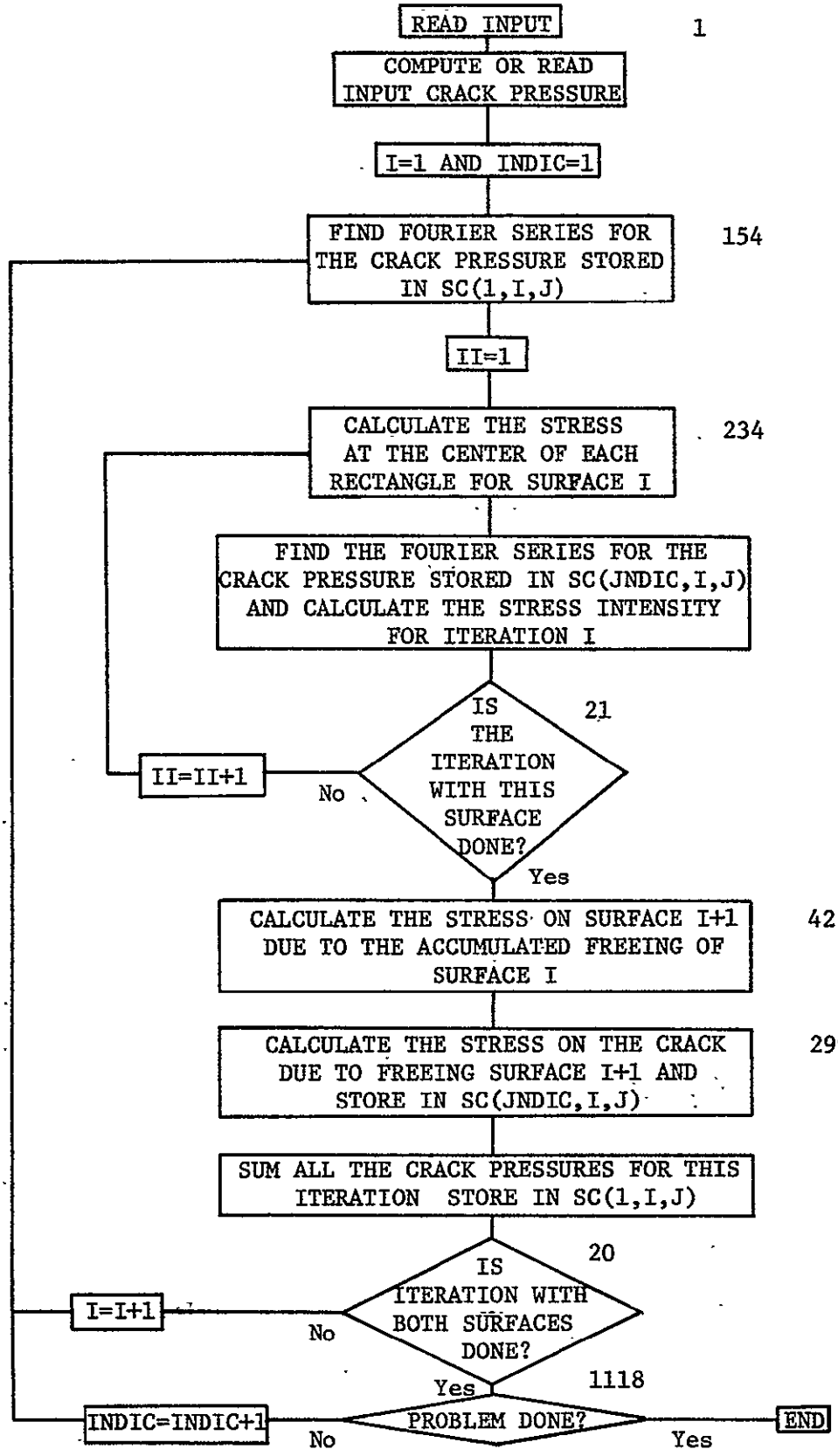

Figure 5.--Block Diagram

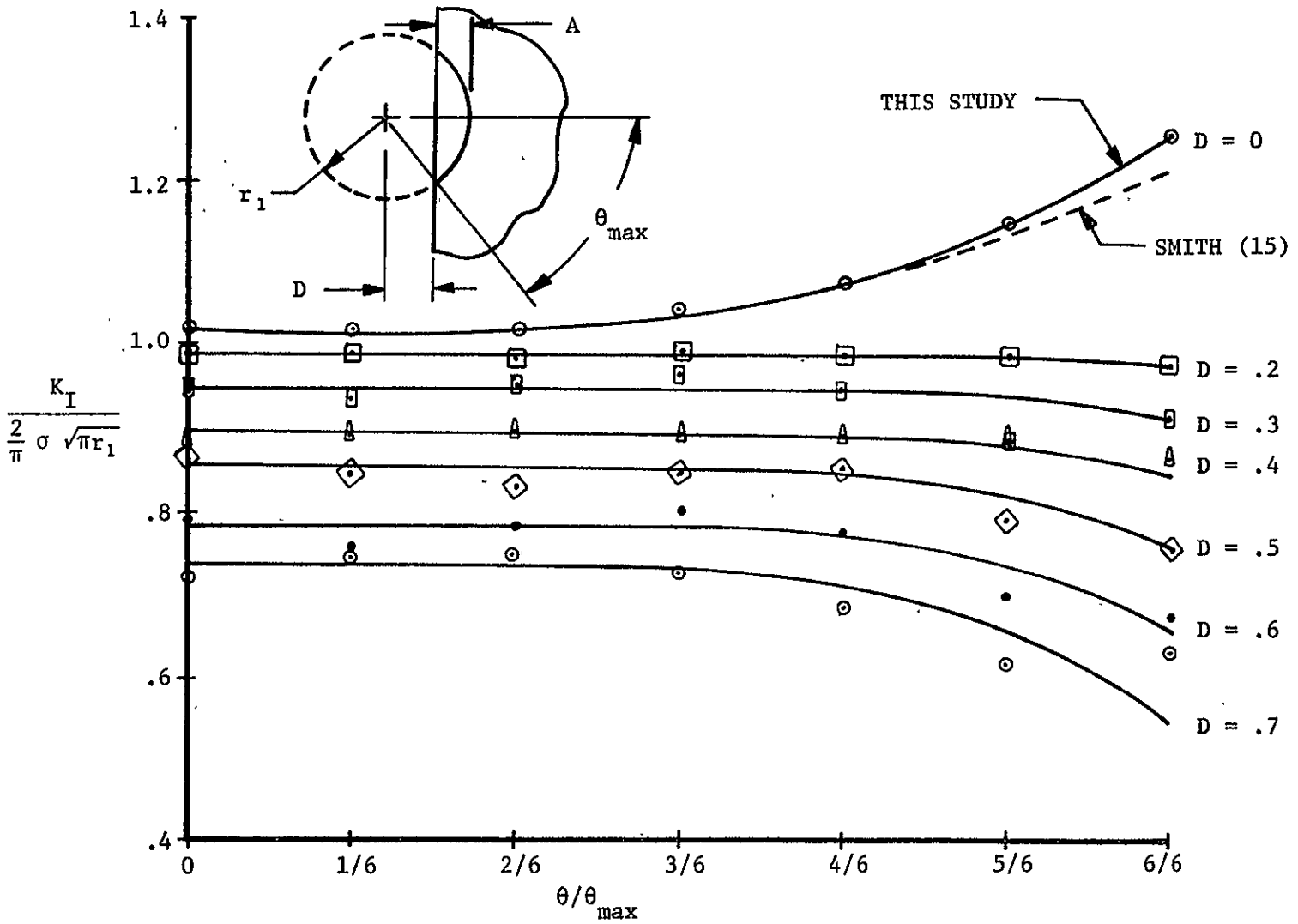

Figure 6.--The Stress Intensity Factor for the Partially Embedded Circular Crack

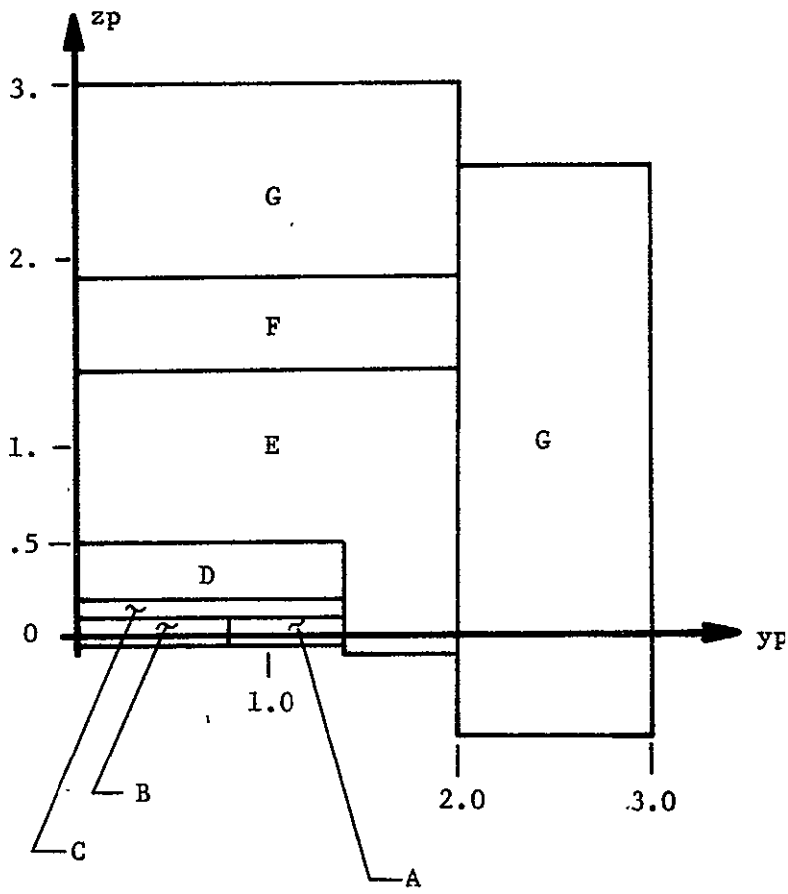

BLOCK	RECTANGLE SIZE Length yp x Length zp
A	.05 x .05
B	.1 x .05
C	.1 x .075
D	.1 x .1
E	.2 x .2
F	.5 x .5
G	1. x 1.

Figure 7.--Front Surface Grid (184 Rectangles)

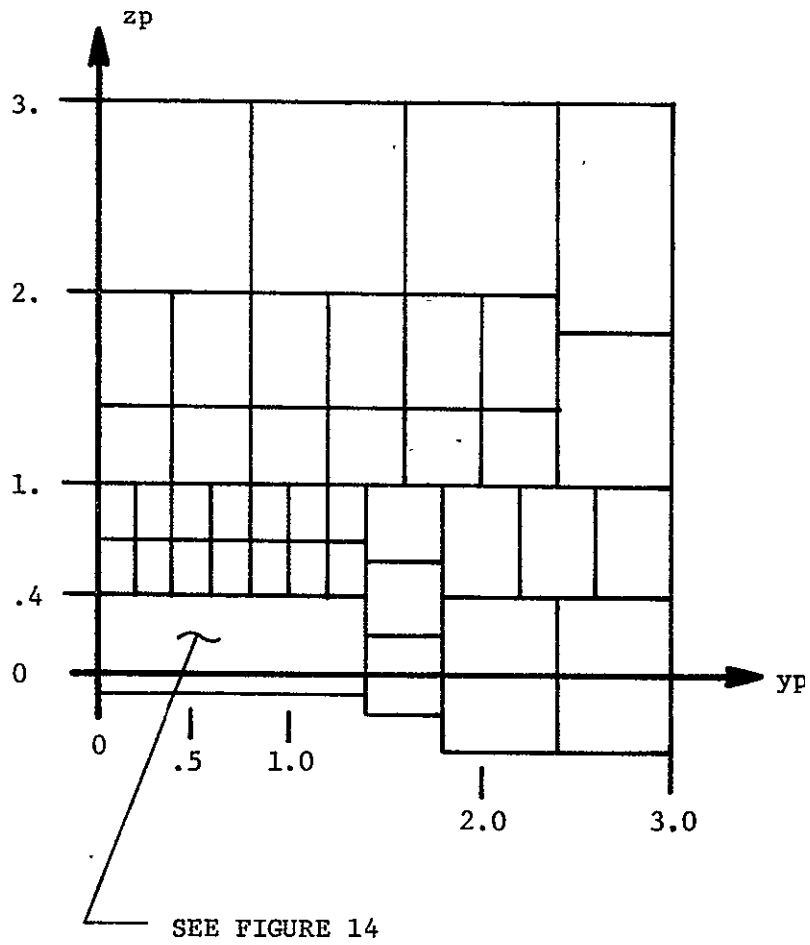

Figure 8.--Front Surface Grid (62 Rectangles)

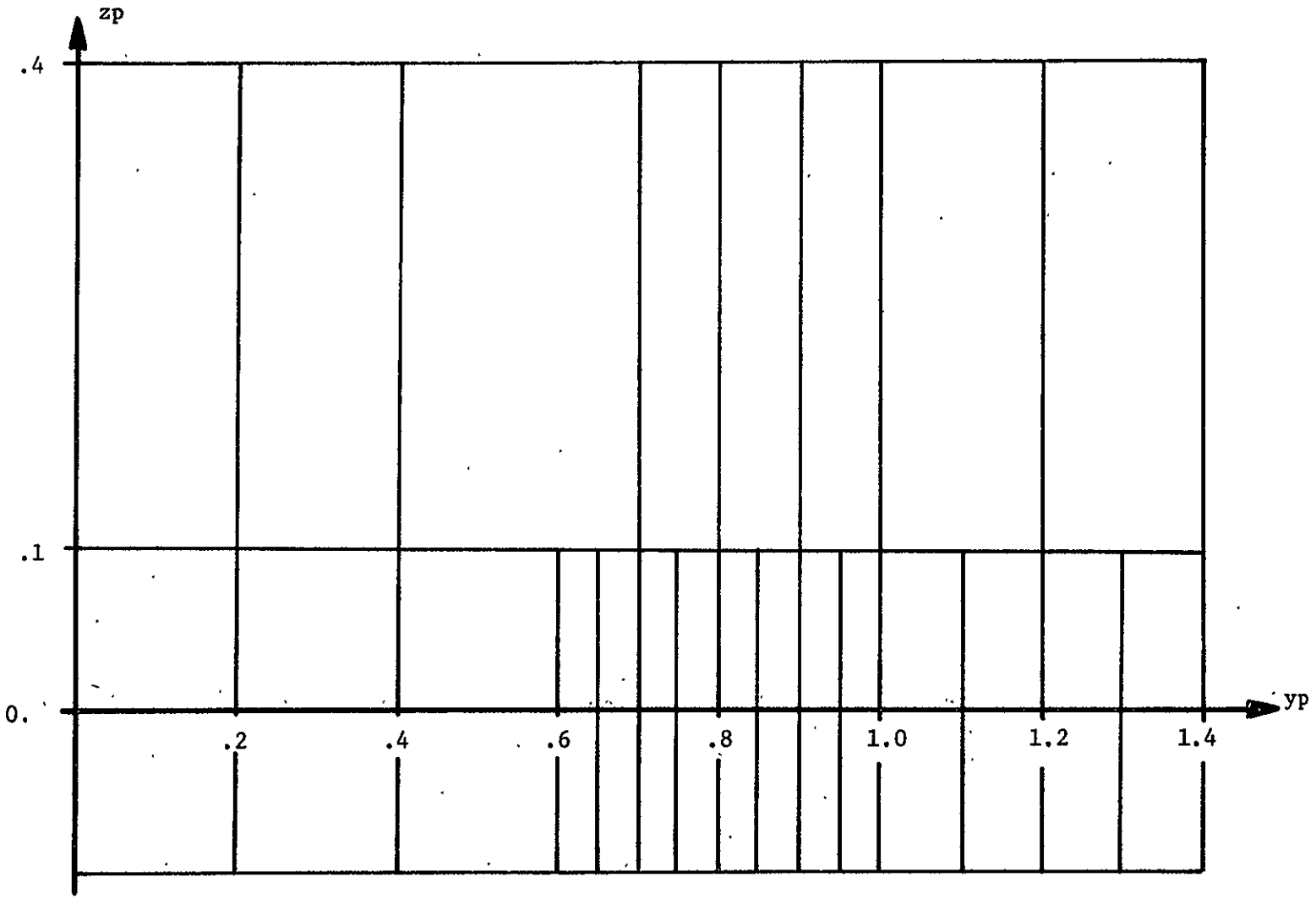

Figure 9.--Front Surface Grid (Detail)

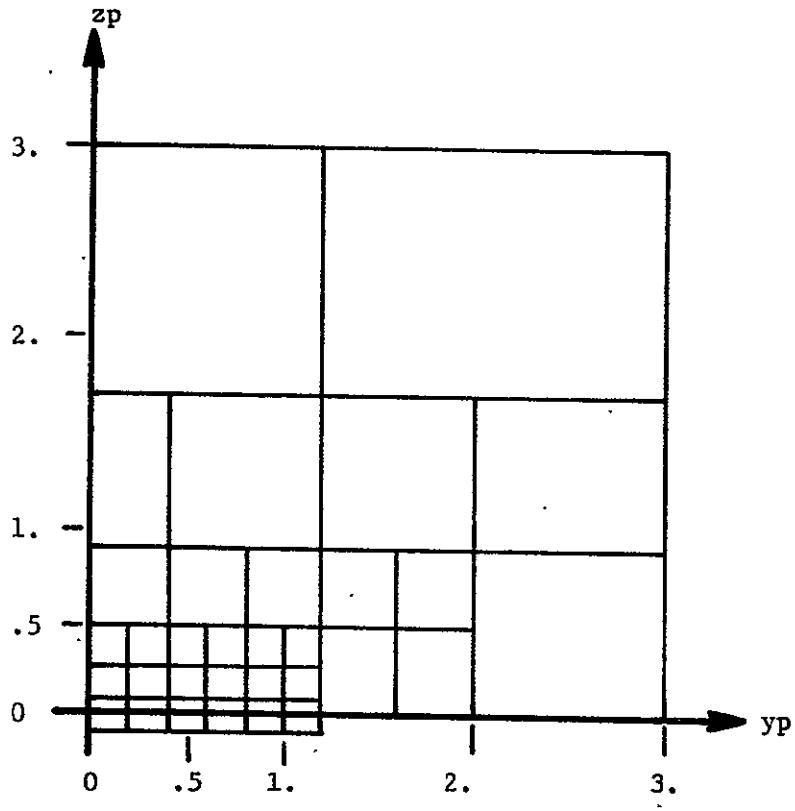

Figure 10.--Back Surface Grid

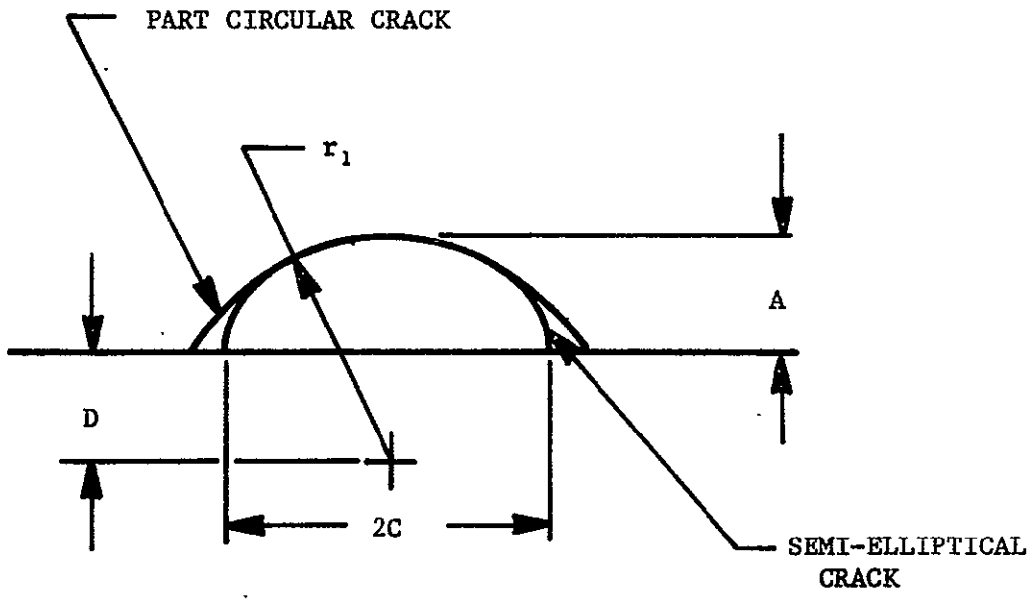

$$A/2C = 1/2 \sqrt{1-D}$$

D	A/2C
0.	.5
.3	.42
.4	.39
.5	.35
.6	.32
.7	.27
.8	.22

Figure 11.--Matching Curvature of the Semi-Ellipse to the Part Circular Crack

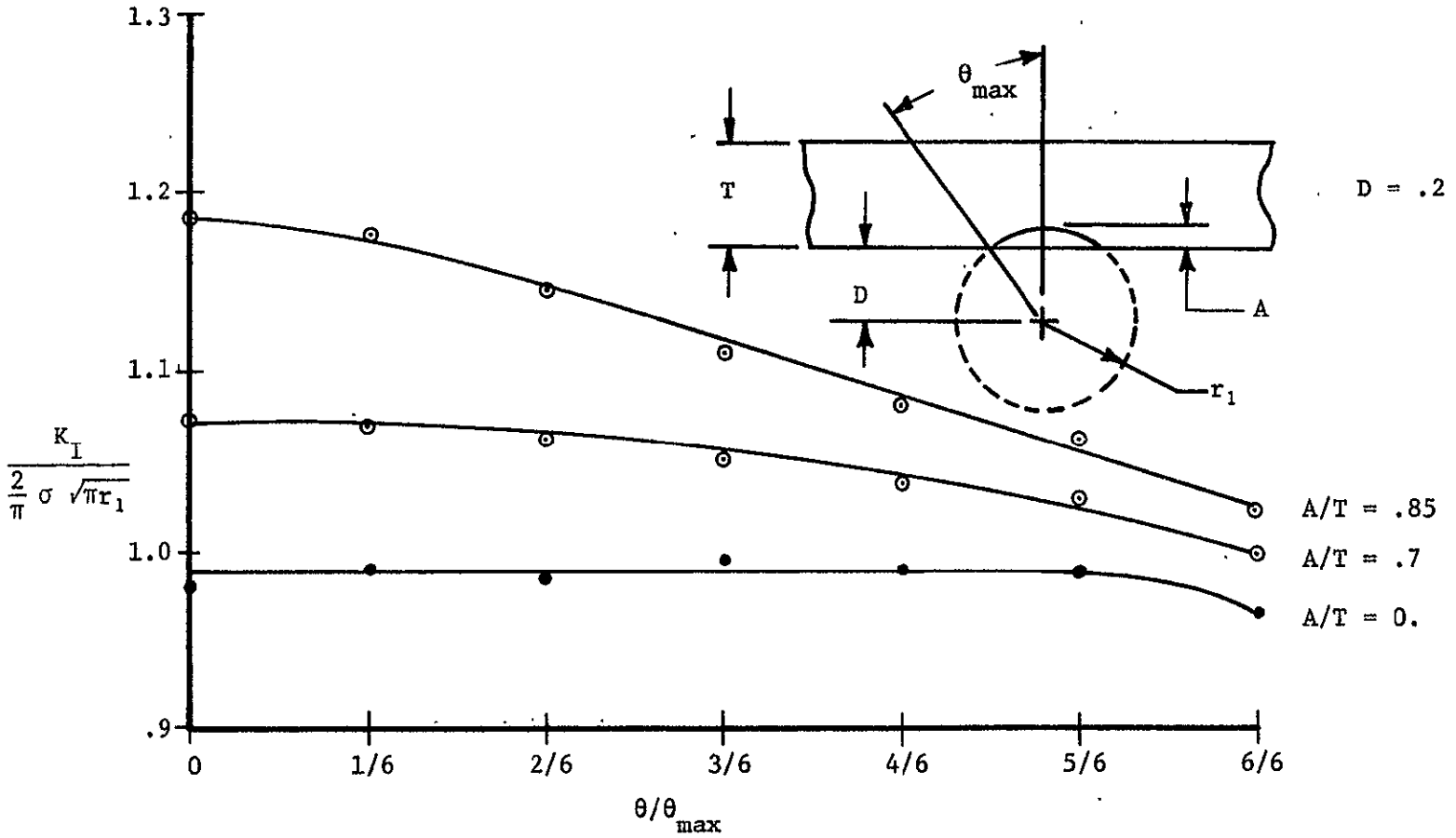

Figure 12.--Back Surface Effect for D = .2

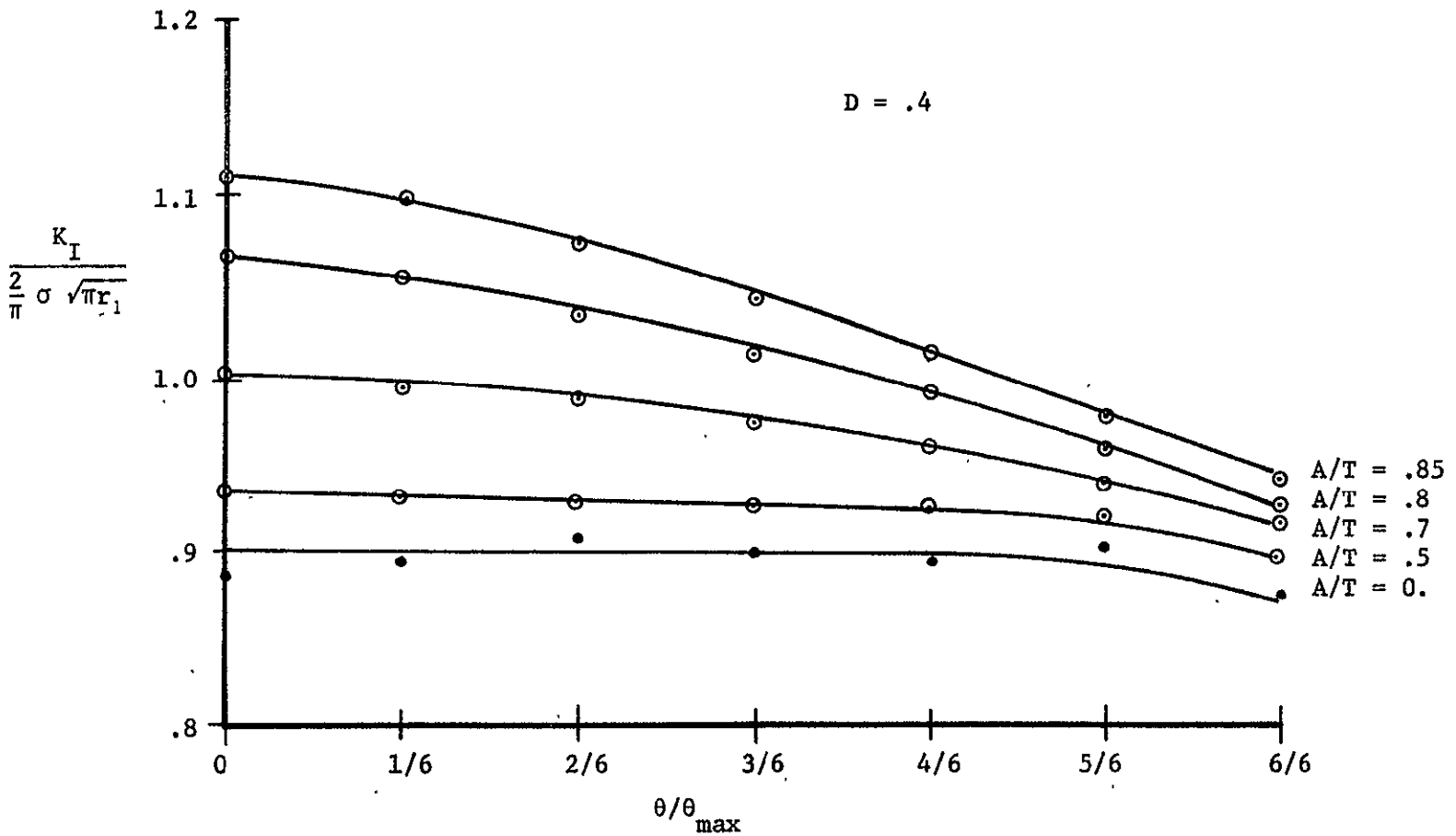

Figure 13.--The Back Surface Effect for D = .4

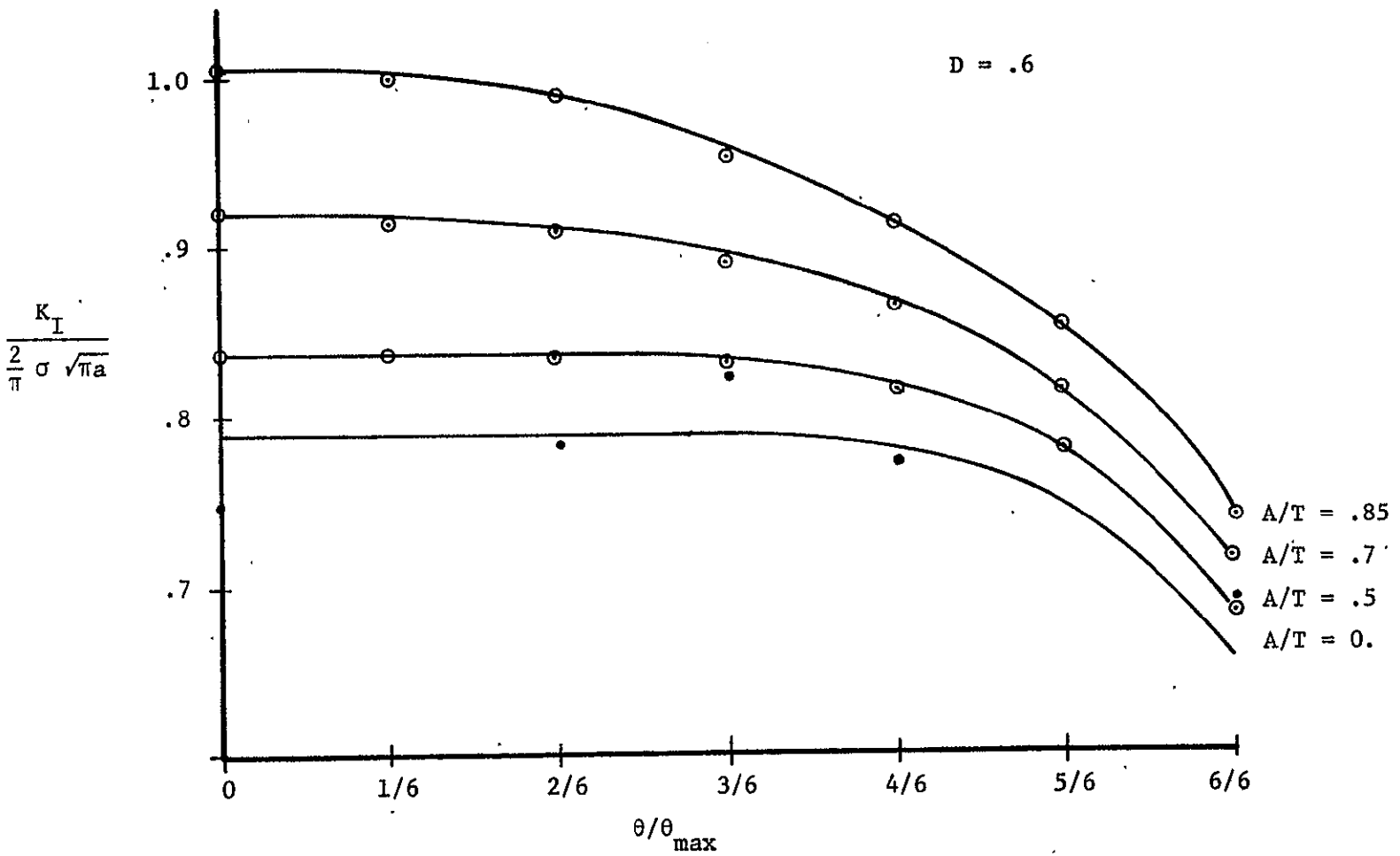

Figure 14.--The Back Surface Effect for D = .6

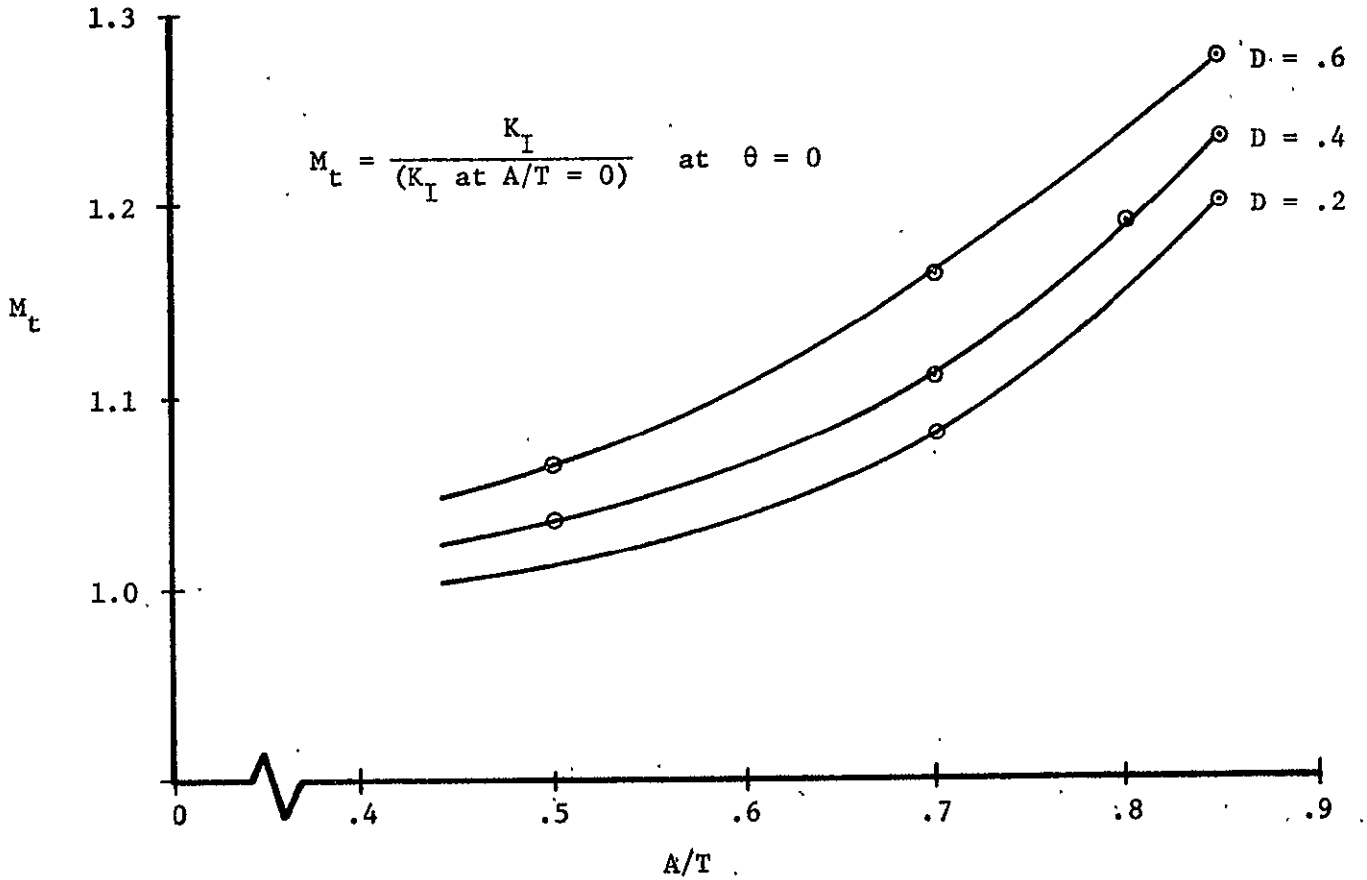

Figure 15.--The Back Surface Intensification

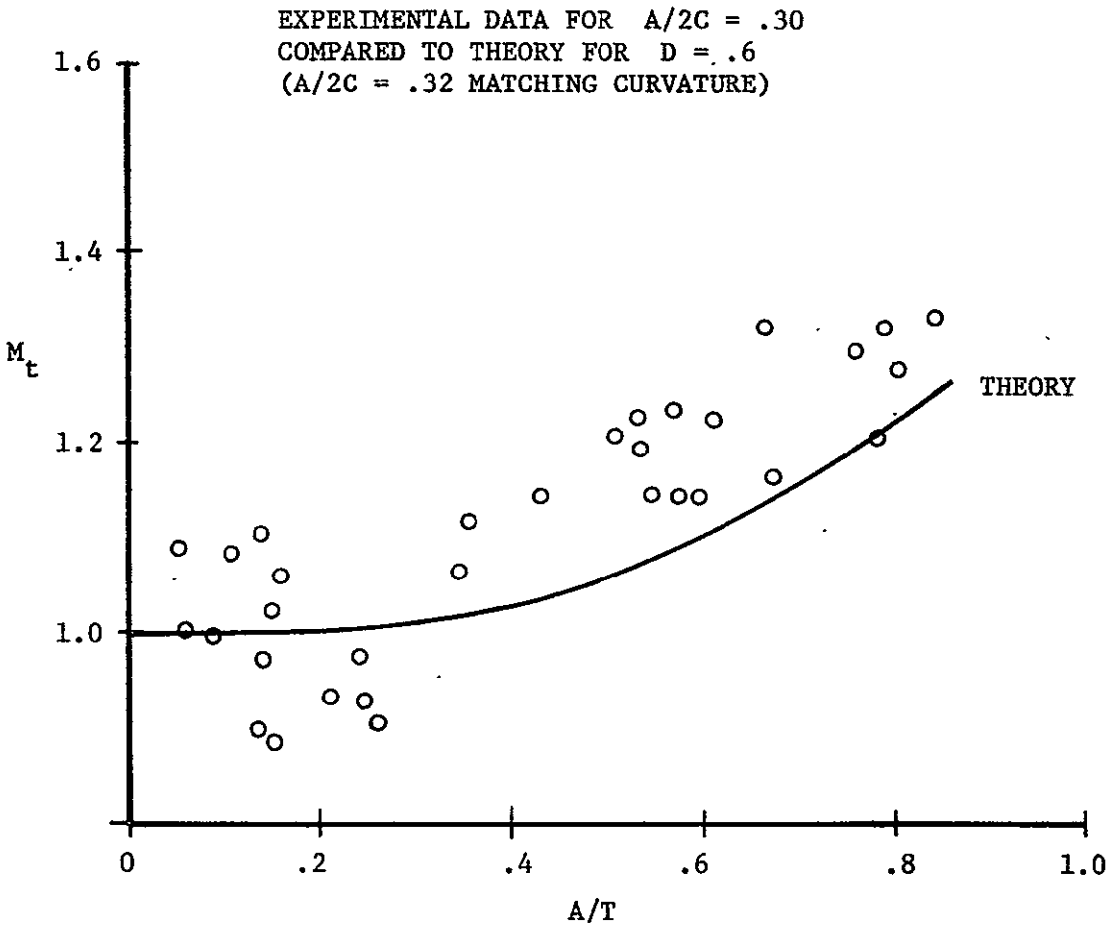

Figure 16.--Comparison with Experimental Data for A/2C = .30

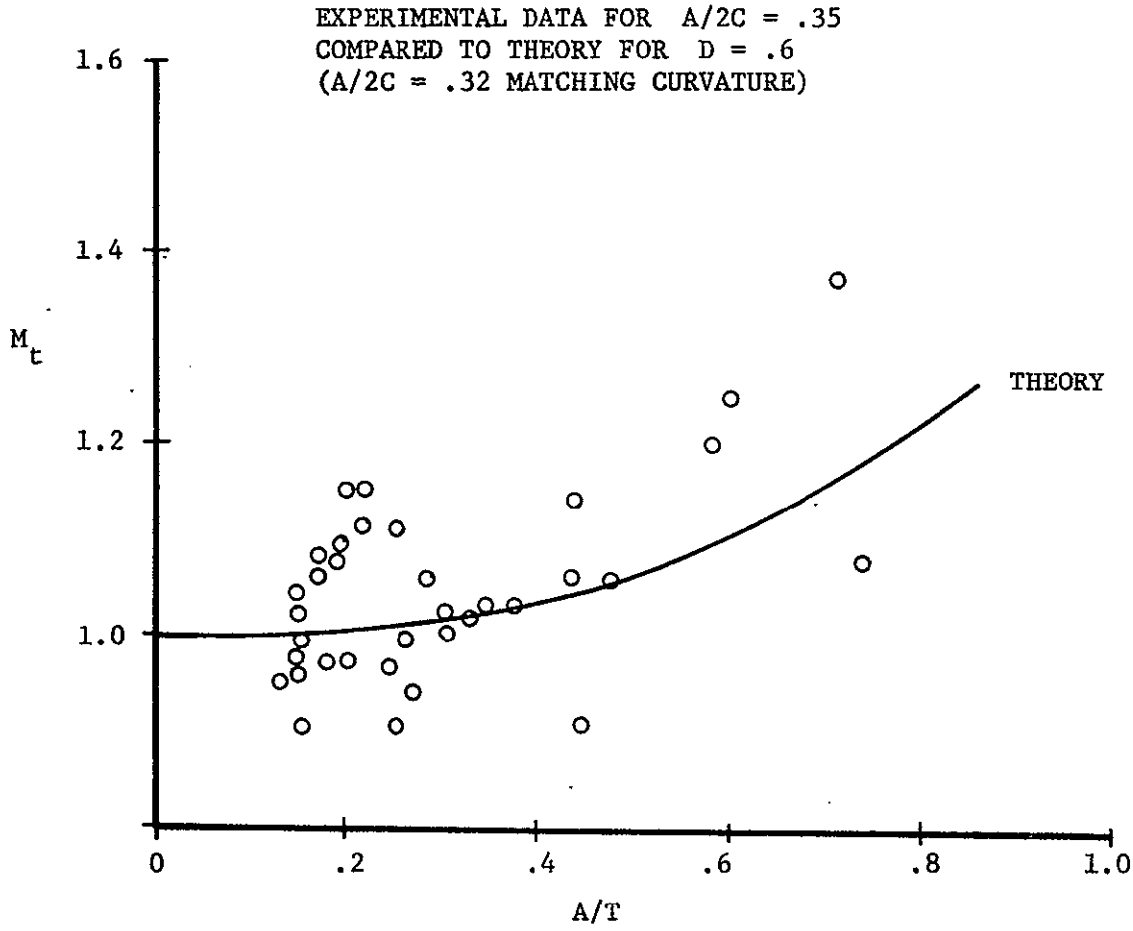

Figure 17.--Comparison with Experimental Data for A/2C = .35

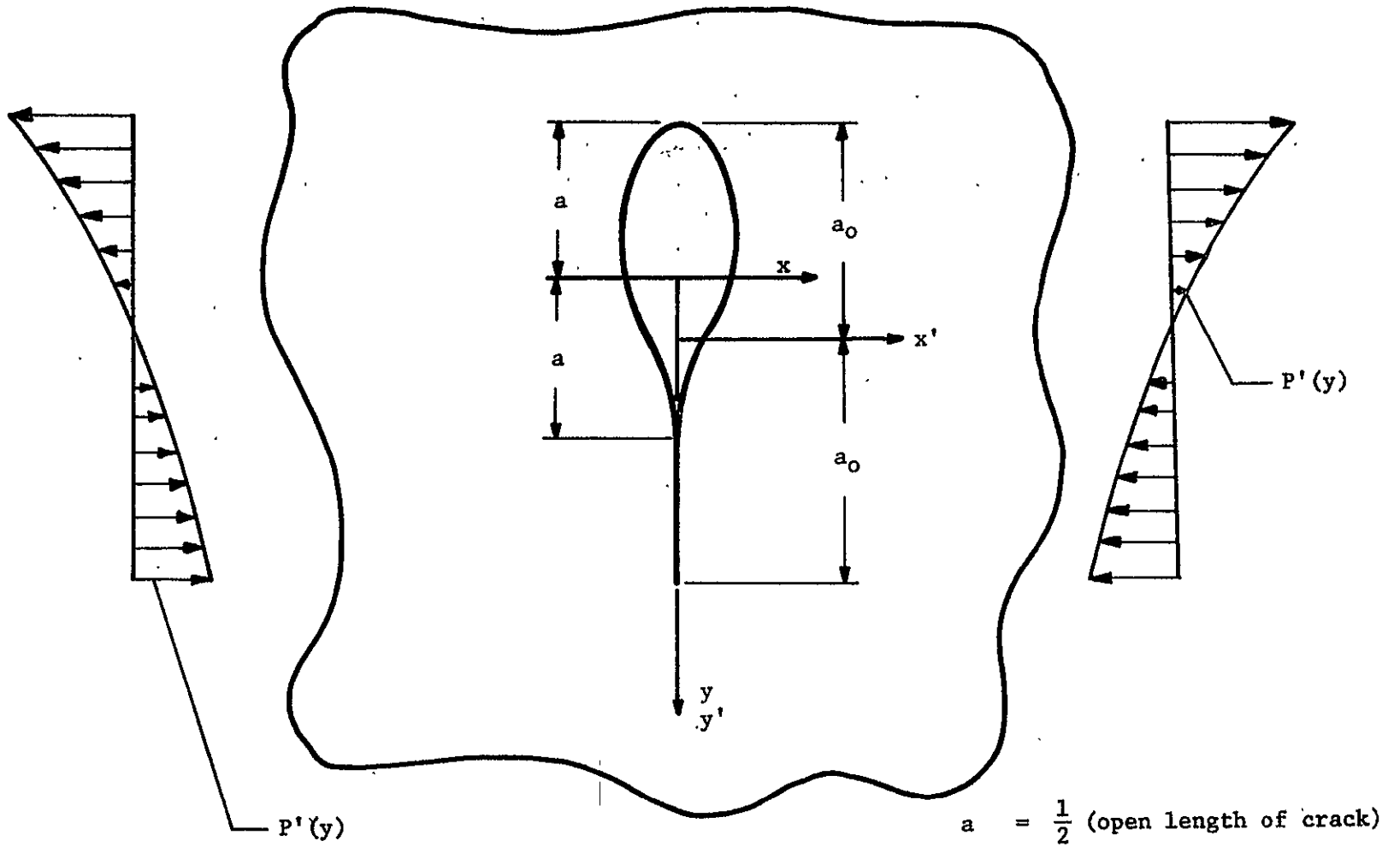

Figure 18.--Problem Geometry

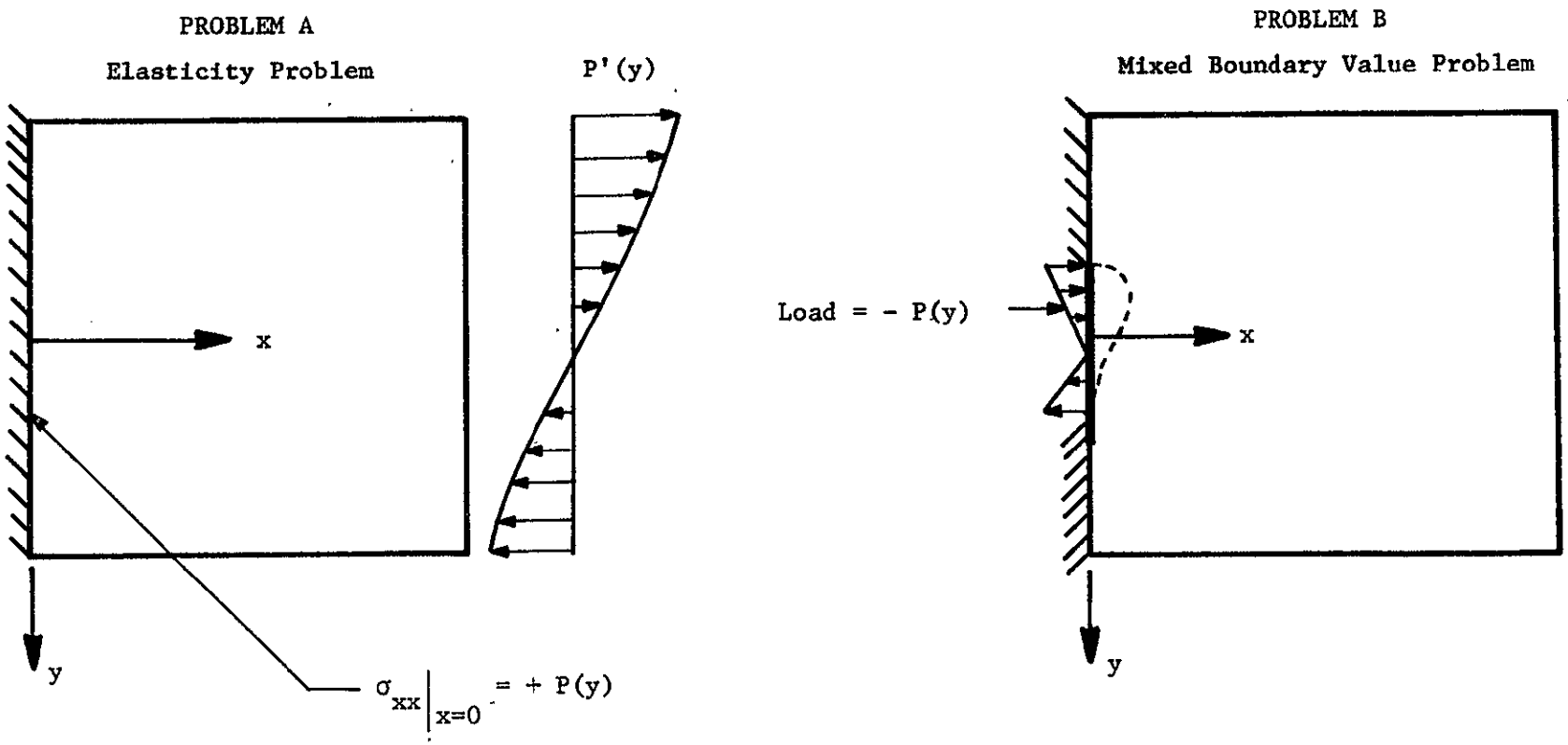

PROBLEM A + PROBLEM B = ORIGINAL PROBLEM

Figure 19.--Superposition

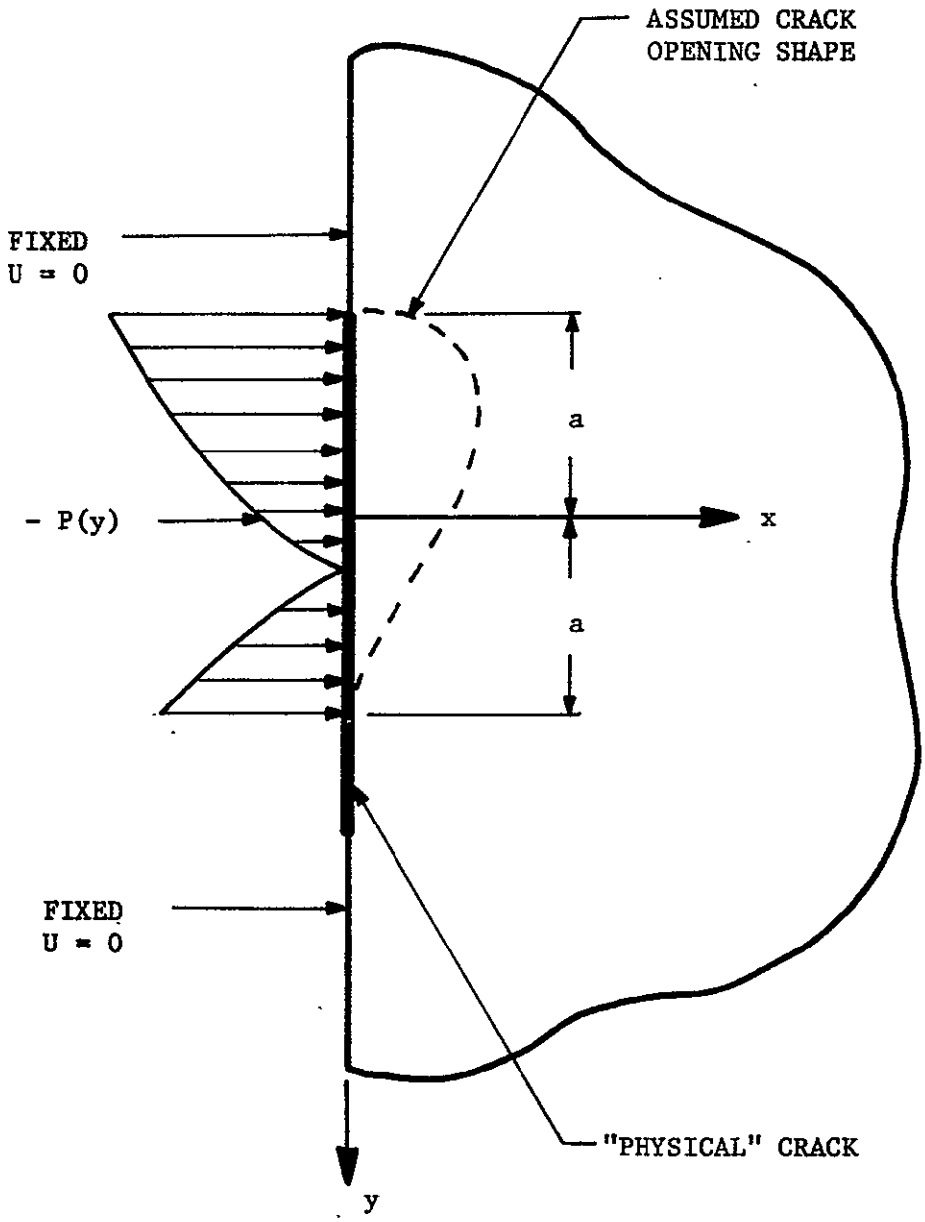

Figure 20.--The Mixed Boundary Value Problem

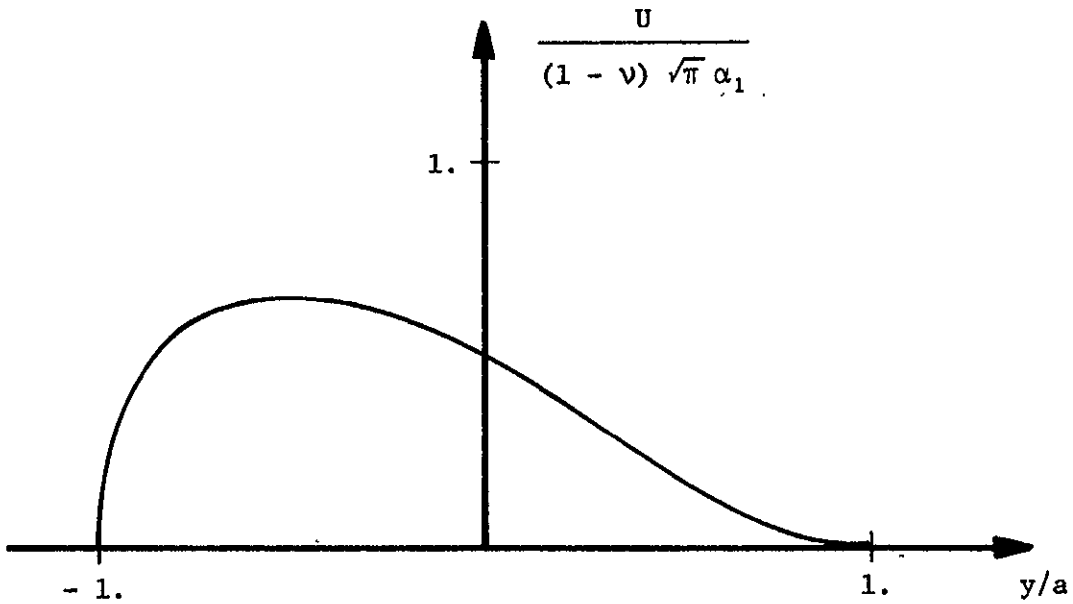

Figure 21.--Crack Opening Displacement

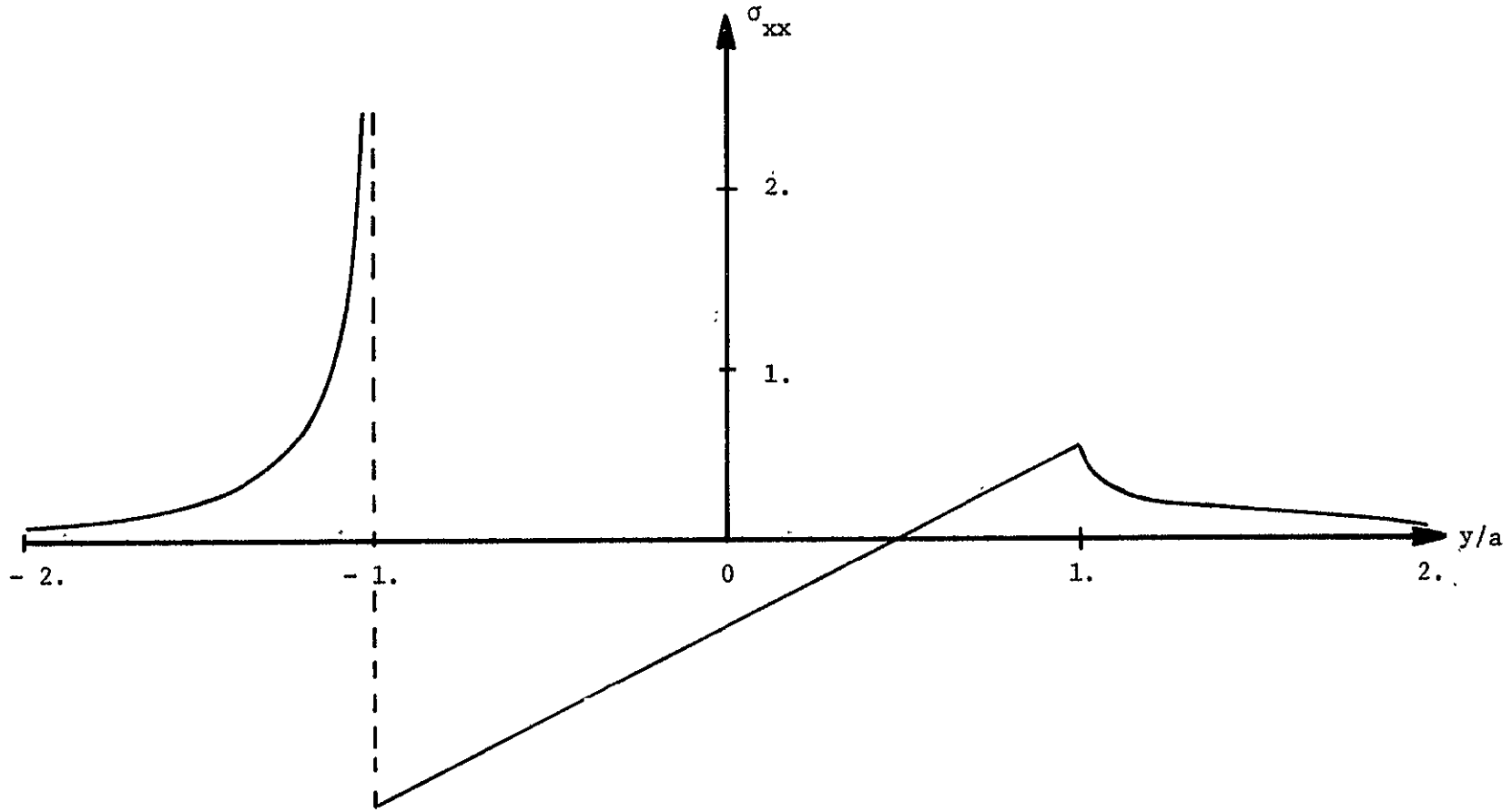

Figure 22.--The Stress on x = 0

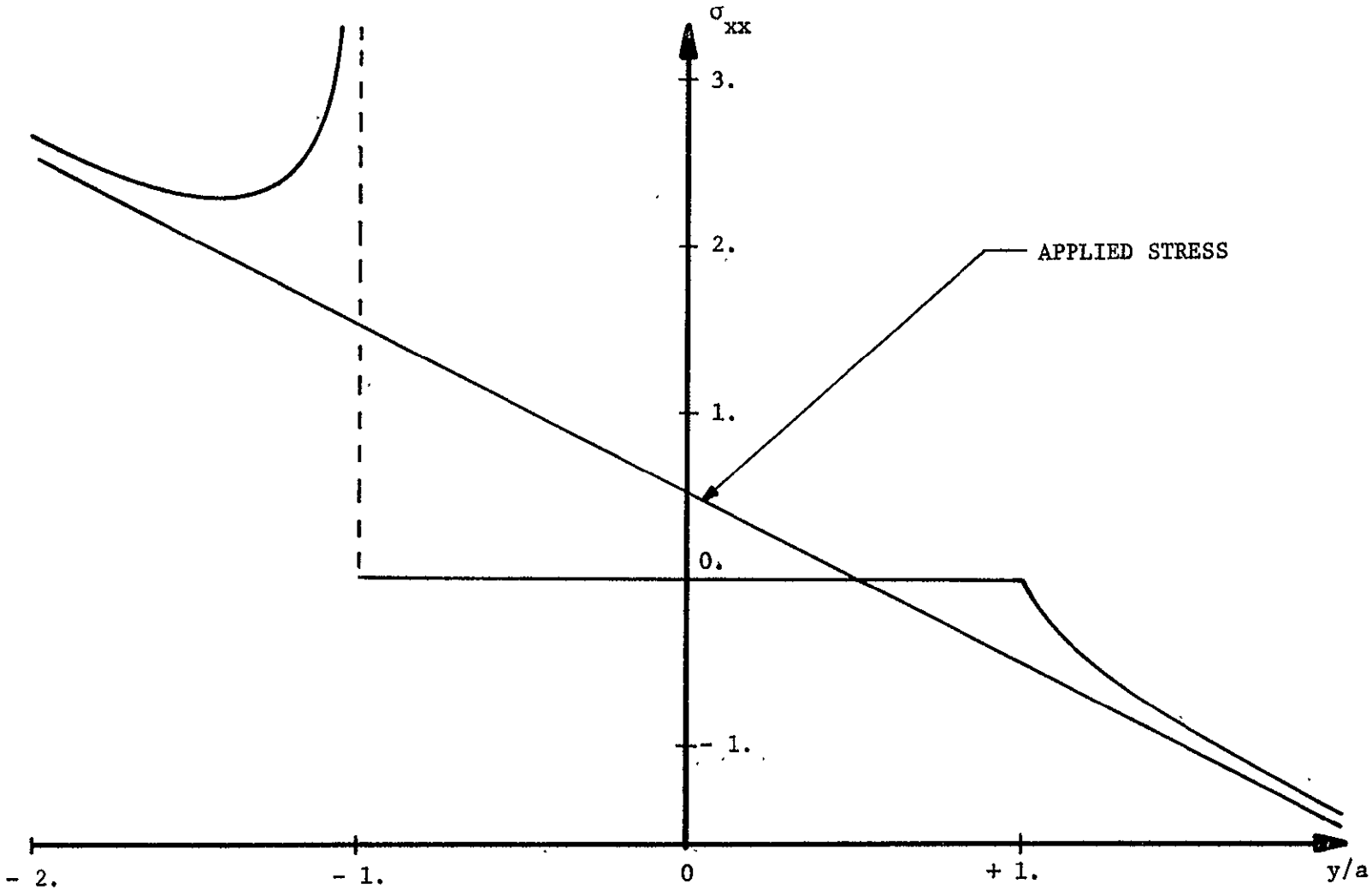

Figure 23.--The Stress for the Original Problem

NOMENCLATURE FOR PART I

σ_{ij} , τ_{ij}	Stress Components
U_i	Displacement Components
$P(r,\theta)$	Crack Pressure
A	Crack Depth
T	Thickness
G	Shear Modulus
ν	Poisson Ratio
λ, μ	Lame´ Constants
β^2	$2(1 - \nu)/(1 - 2\nu)$
ϕ	Potential Function
B_n	Fourier Coefficients
C_n^p	Power Series Coefficients
$J_\nu(z)$	Bessel Function of the first kind of order ν
H_n^p	$\Gamma(\frac{p+n+2}{2})/\Gamma(\frac{p+n+3}{2})$
K_I	Stress Intensity Factor
D	Depth of Circular Crack
r, θ, z	Circular Cylindrical Coordinates
x, y, z	Rectangular Cartesian Coordinates
δ	Distance from the Crack Tip
a , r_1	Crack Radius

NOMENCLATURE FOR PART II

σ_{ij} , τ_{ij}	Stress Components
U	x Displacement
V	y Displacement
a	Length of Open Portion of the Crack
a_o	Physical Crack Length
P'(y)	Load on the Infinite Space
P(y)	Load on the Crack Surface
ν	Poisson Ratio
β^2	$2(1 - \nu)/(1 - 2\nu)$
G	Shear Modulus
ϕ	Potential Function
$P_s(y)$	Symmetric Portion of P(y)
$P_a(y)$	Anti-symmetric Portion of P(y)
α_n	Loading coefficients for the Polynomial P'(y)
β_m	Loading Coefficients for the Polynomial P(y)
$J_\nu(z)$	Bessel Function of the first kind of order ν
K_I	Stress Intensity Factor
x , y	Two Dimensional Rectangular Cartesian Coordinates
δ	Distance from the Crack Tip

LIST OF REFERENCES

(1) Griffith, A. A., "The phenomena of rupture and flow in solids." Philosophical Transactions, Royal Soc. (London), Series A., Vol. 221, 1920, pp. 163-198.

(2) Inglis, C. E., "Stresses in a plate due to the presence of cracks and sharp corners." Transactions, Inst. Naval Architects, Vol. 60, 1913, p. 219.

(3) Irwin, G. R., "Fracture dynamics." Fracturing of Metals, Am. Soc. Metals, Cleveland, 1948, pp. 147-166.

(4) Irwin, G. R., "Analysis of stress and strain near the end of a crack." Journal of Applied Mechanics, Vol. 24, 1957, pp. 361.

(5) ASTM No. 381, "Fracture toughness testing and its applications." American Society for Testing and Materials, Philadelphia, Pa., 1964.

(6) Sneddon, I. N., "The distribution of stress in the neighborhood of a crack in an elastic solid." Proceedings of the Royal Society (London), Series A, Vol. 187, 1946.

(7) Green, A. E., and I. N. Sneddon, "The distribution of stress in the neighborhood of a flat elliptical crack in an elastic solid." Proceedings of the Cambridge Philosophical Society, Vol. 46, 1960, pp. 159-163.

(8) Kassir, M. K., and G. C. Sih, "Three dimensional stress distribution around an elliptical crack under arbitrary loading." Journal of Applied Mechanics, Transactions of ASME, Sept. 1966.

(9) Kassir, M. K., and G. C. Sih, "Geometric discontinuities in elastostatics." Journal of Mathematics, Vol. 16, No. 9, 1967.

(10) Shaw, R. C., "Stresses and stress intensity factors for embedded hyperbolic and parabolic cracks." Ph.D. Thesis, University of Washington, 1966.

(11) Shaw, R. C., and A. S. Kobayashi, "Stress intensity factor for an elliptical crack under arbitrary normal loading." Submitted for publication.

(12) Irwin, G. R., "Crack extension force for a part through crack in a plate." Journal of Applied Mechanics, Dec. 1966.

(13) Smith, F. W., "Stresses near a semi-circular edge crack." Ph.D. Thesis, University of Washington, 1966.

(14) Alavi, M. J., "Stresses near a circular crack in a half space." Ph.D. Thesis, Colorado State University, 1968.

(15) Smith, F. W. and M. J. Alavi, "Stress intensity factors for a penny-shaped crack in a half space." To be published in the Journal of Engineering Fracture Mechanics. Presented at Lehigh University, August, 1969.

(16) Smith, F. W. and M. J. Alavi, "Stress intensity factors for a part-circular surface flaw." Proceedings of the 1st International Pressure Vessel Conference, Delft, Holland, Oct. 1969.

(17) Kantorovich, L. V. and V. I. Kuylov, "Approximate methods of higher analysis." Wiley, New York, 1964.

(18) Green, A. E. and W. Zerna, "Theoretical elasticity." Oxford at the Clarendon Press, 1960.

(19) Sneddon, I. N., "Fourier transforms." McGraw-Hill, New York, 1951.

(20) Watson, G. N., "A treatise on the theory of Bessel functions." New York, the MacMillan Co., 1944.

(21) Abramowitz, M. and I. A. Stegun, "Handbook of Mathematical functions." National Bureau of Standards, Applied Mathematics, Series 55, 1965.

(22) Love, A. E. H., "A treatise on the mathematical theory of elasticity." Dover, New York, 1944.

(23) Love, A. E. H., "On stress produced in a semi-infinite solid by pressure on part of the boundary." Philosophical Transactions of the Royal Society, A, Vol. 228, 1929.

(24) Smith, F. W., "Stress intensity factors for a semi-elliptical surface flaw." Structural Development Research Memo., No. 17, The Boeing Company, August 1966.

(25) Larson, L. J., "Depth effect for semi-elliptical surface flaws." Masters Thesis, Colorado State University, August 1968.

(26) Borniston, E. E., "An example of a partially closed Griffith crack." International Journal of Fracture Mechanics, Vol. 5, No. 1, March 1969, p. 17.

(27) Sneddon, I. N., "Crack problems in the mathematical theory of elasticity." Technical Report No. 486(06), North Carolina State College University, Raleigh, 1961.

(28) Emery and Smith, "Some basic properties of penny-shaped cracks." Mathematika 13 (1966), pp. 172-180.